

Emergency Index (EI): A Two-Dimensional Surrogate Safety Measure Considering Vehicles' Interaction Depth

Hao Cheng^a, Yanbo Jiang^a, Hailun Zhang^a, Keyu Chen^a, Heye Huang^b, Shaobing Xu^a, Jianqiang Wang^a, Sifa Zheng^{a,*}

^aSchool of Vehicle and Mobility, Tsinghua University, Beijing, 100084, China

^bDepartment of Civil and Environmental Engineering University of Wisconsin-Madison Madison, WI, 53706, USA

Abstract

Surrogate Safety Measures (SSMs) are pivotal in road safety due to their efficiency and effectiveness in vehicle risk assessment. However, traditional SSMs, such as Time-to-Collision (TTC), face challenges in addressing multi-angle conflicts in a two-dimensional (2D) plane. Although some 2D-SSMs can resolve the aforementioned issue, they still have three limitations: (i) incomplete preconditions of SSMs can lead to missed vehicle conflicts; (ii) extending TTC-based logic to a 2D plane may result in optimistic risk estimates; (iii) lack of accurate consideration for the necessary state adjustments of evasive maneuvers. To address these challenges, this paper proposes a novel SSM called the Emergency Index (EI), introducing an innovative framework that integrates complex conflict relationships into an intuitive and interpretable risk assessment model. EI utilizes the concept of Interaction Depth (InDepth), defined as the maximum depth at which two vehicles are projected to intrude into each other's safety region, representing the necessary adjustments for pre-collision states. The physical significance of EI lies in the rate of change in InDepth required for evasive actions, offering unique insights into crash avoidance strategies. Additionally, this paper introduces a Conflict Detection Model (CDM) to comprehensively screen potential conflict vehicles. Simulations and driving simulator experiments under various conflict types reveal that: (i) our proposed CDM reduces the occurrence of undetected conflicts; (ii) EI accurately reflects the impact of evasive maneuvers on risk. Further, this paper uses real vehicle crash-conflict datasets to validate the binary classification performance on conflict/collision events through the ROC-AUC method. The results show the superiority of EI in risk assessment, compared to six other classical SSMs. Finally, we tested EI on the complex interaction dataset SinD in real-time safety monitoring scenarios, demonstrating its potential as an effective method for enhancing road safety.

Keywords: Surrogate safety measures, Vehicle conflict, Road safety, Risk assessment, Collision avoidance

1. Introduction

Road traffic accidents are a major public health issue (Tselentis & Papadimitriou, 2023), claiming about 1.35 million lives and injuring over 50 million people annually (Organization, 2019). Many researchers and organizations are focused on assessing and mitigating the risks linked to road fatalities (Xie et al., 2019; Nikolaou et al., 2023). Among them, extracting and analyzing safety-critical events is an important way to evaluate road safety. Traditional methods rely on historical crash data. However, since the occurrence probability of accidents is extremely low, it is unrealistic to obtain adequate crash data for statistical analysis in the short term (Scanlon et al., 2021). Surrogate Safety Measures (SSMs) have been recognized as a better proactive surrogate approach for analyzing traffic safety issues (Tafidis & Pirdavani, 2023). SSMs have the following potential (Arun et al., 2021): (i) they can capture the more frequent 'near-crash' situations and improve efficiency; (ii) they take into account driving behaviors in the assessment of vehicle collision risks; and (iii) they provide deeper insight into the mechanisms and sequences of events that cause road traffic collisions and their subsequent impacts. However, traditional SSMs, such as Time-to-

* Corresponding author

Email addresses: chengh22@mails.tsinghua.edu.cn (Hao Cheng), jyb23@mails.tsinghua.edu.cn (Yanbo Jiang), Iszhanghailun@outlook.com (Hailun Zhang), chenky23@mails.tsinghua.edu.cn (Keyu Chen), hhuang468@wisc.edu (Heye Huang), shaobxu@tsinghua.edu.cn (Shaobing Xu), wjqlws@tsinghua.edu.cn (Jianqiang Wang), zsf@tsinghua.edu.cn (Sifa Zheng)

Collision (TTC), are limited by their application scenarios and face challenges in addressing multi-angle conflicts in a 2D plane.

In recent years, some SSMs that combine metrics (Guo et al., 2023) or extend through vectorization (Ward et al., 2015; Venthuruthiyil & Chunchu, 2022) have emerged, attempting to quantify the risks of vehicle conflicts in all forms within two-dimensional (2D) spaces and have achieved preliminary application results. These methods typically involve two steps: (1) detecting potential conflicts through a set of predefined “preconditions”; (2) calculating the risk values. The preconditions serve as a filtering mechanism for potential conflicts in these SSMs, reflecting the fundamental definitions of conflicts in different SSMs. However, the preconditions for 2D-SSMs should not exhibit a preference for specific conflict types. The validity and comprehensiveness of these preconditions are often overlooked, potentially leading to missed conflict detections. In terms of risk quantification, most 2D-SSMs directly use the TTC calculation logic in a 2D plane. These methods mainly focus on the remaining time before the geometric centers of two vehicles converge in a certain direction, which differs from the actual collision time and may lead to an optimistic estimate of proximity. Additionally, while these methods are suitable for 2D situations, they essentially measure proximity in a single closure direction at each instant. However, this single-directional proximity cannot effectively capture the intensity required for multiple forms of evasive actions. On the other hand, the effectiveness of these SSMs in various forms of conflict has not been sufficiently validated, especially with extensive real-world road conflict and crash data. To date, there is still a lack of an indicator that effectively explains the mechanisms of accident evolution in a 2D plane. Ideally, such an indicator should not only consider temporal-spatial proximity but also accurately represent the difficulty of avoiding collisions within a 2D plane, with clear physical significance.

The focus of this paper is to reveal the mechanisms of 2D vehicle conflict risks from a new perspective. We introduce a 2D-SSM framework comprising two components: conflict detection and risk quantification. The conflict detection component is capable of real-time detection and updating of the set of potentially conflicting vehicle pairs. The risk quantification component aims to assess the collision risks of vehicle pairs with potential conflicts of any type and seeks to accurately reflect the impact of evasive maneuvers on risk.

The main contributions of this paper include:

1. We propose the Conflict Detection Model (CDM) as a new method for efficiently extracting valuable interactions between road users. CDM transforms the qualitative conditions of conflict definition into a formalized judgment method, consisting of two mathematical criteria that emphasize the importance of vehicle body geometry in detecting close-range conflicts. The CDM can effectively reduce missed detections and can be used as a universal precondition for SSMs.
2. We propose the Emergency Index (EI), which integrates a multitude of conflict relationships within an interpretable risk assessment framework, indicating the urgency of necessary evasive actions. EI incorporates the concept of Interaction Depth (InDepth), which indicates the necessary state adjustments of evasive maneuvers between vehicle pairs. The physical meaning of EI lies in the rate at which InDepth needs to change for evasive actions. EI transcends the limitations of classical SSMs that rely on single-direction proximity measurements, offering a new framework for 2D-SSMs.

The rest of this paper is organized as follows. In Section 2, a thorough literature review of the related research is carried out. Section 3 describes the methodology of the proposed CDM and EI. Section 4 presents the performance evaluation of EI. Finally, the conclusions are summarized in Section 5.

2. Related Works

Most SSMs measure the proximity to collision, while some focus on the crash severity (Arun et al., 2021). This paper centers on SSMs applicable to active safety analysis, specifically the former. In some literature, these proximal SSMs are referred to as SSMs that evaluate “conflict severity” or “severity of interactions” (Mahmud et al., 2017; Wang et al., 2021). For each proximal SSM, we consider it to consist of two components: (1) the definition of conflict, i.e., preconditions; (2) the understanding of risk, i.e., the calculation method. In this section, we first review the proximal SSMs previously proposed and then introduce their preconditions.

2.1. Surrogate Safety Measures

The most widely applied SSMs are time-based SSMs, which have the advantage of combining spatial proximity and velocity (Zheng et al., 2014). TTC is the most representative among them, defined as the remaining time until a potential collision, given the constant speed and direction of the interacting vehicles (Hayward, 1972).

Extensions of the TTC concept include Time Exposed TTC (TET) (Minderhoud & Bovy, 2001), Time Integrated TTC (TIT), Time-to-Lane Crossing (TLC) (Van Winsum et al., 2000), and Modified TTC (MTTC) (Ozbay et al., 2008). Another classic time-based SSM is Post-encroachment Time (PET), which is defined as the time between one road user leaving a point (or conflict area) and another road user arriving at the same location (Allen et al., 1978). Thus, PET has a single value for a given event. Time Advantage (TAdv) extends the concept of PET, providing real-time risk representation by estimating the value of PET at each moment assuming the vehicle continues with the same speed and path (Laureshyn et al., 2010). Although many types of SSMs have been proposed and each has its respective applicable scenarios, there is still no consensus on which indicators should be prioritized under specific circumstances. (Ismail et al., 2011; Salamat et al., 2011; Arun et al., 2021).

Apart from temporal indicators, SSMs based on evasive actions have also gained significant attention for their effectiveness in quantifying the difficulty of performing evasive maneuvers. One of the most commonly used evasive action-based SSMs is the Deceleration Rate to Avoid the Crash (DRAC), which is defined as the differential speed between a following vehicle and its lead vehicle, divided by their closing time (Almqvist et al., 1991). Its limitation, however, lies in its applicability being restricted to longitudinal car-following situations. Cunto (2008) developed the Crash Potential Index (CPI), which represents the probability that DRAC at a given moment exceeds the Maximum Allowable Deceleration Rate (MADR). The Proportion of Stopping Distance (PSD) has potential for various conflict types, defined as the ratio between the remaining distance to the potential point of collision and the minimum acceptable stopping distance (Astarita et al., 2012). However, it only considers single-vehicle braking behavior. The Criticality Index Function (CIF) considers two assumptions (Chan, 2006): (i) higher collision speeds lead to more severe consequences, and (ii) a longer time for evasive maneuvers increases the probability of avoiding a collision. However, CIF quantifies risk based solely on relative speed and TTC, which makes it applicable only to longitudinal scenarios. Overall, existing evasive-based SSMs only consider braking maneuvers by a single vehicle and are primarily used in car-following scenarios. In 2D situations, evasive actions can be longitudinal, lateral, or a combination of both. Additionally, evasive maneuvers can be executed by either vehicle independently or as a coordinated action by both vehicles. How to integrate various forms of evasive action and any party involved in evasive maneuvers into a unified risk assessment framework is an area worth exploring.

In recent years, driven by the increasing need to represent the risks of complex interactions, several studies have proposed SSMs for 2D vehicle conflicts. There are mainly two approaches: combining metrics and using vectorized calculations of TTC. Firstly, the combination method, Laureshyn et al. (2010) suggested combining TTC with TAdv to smoothly assess the transition collision risks between rear-end and angle conflicts. Guo et al. (2023) introduced a concept of 2D-TTC, where TTC is calculated separately in longitudinal and lateral directions and the smaller value is used. This method has initially been verified in lane-changing scenarios. Tang et al. (2024) introduced the potential conflict risk index (PCRI), which integrates three different indicators into a risk assessment framework for analyzing conflicts in highway merging areas. However, the combining metrics approach, which integrates different SSMs into a hierarchical risk framework, may pose challenges to interpretability and credibility. Next, the vectorized expansion method for TTC, Hou et al. (2014) proposed an algorithm that calculates TTC by solving a 2D distance equation and validates these algorithms with simulation models. Ward et al. (2015) presented the Extended Time-to-Collision (ETTC), using vector methods to calculate the collision time for vehicles in unconstrained motion. Xing et al. (2019) utilized ETTC to assess the collision risk of unconstrained vehicles in toll plaza areas. Venthuruthiyil & Chunchu (2022) proposed the Anticipated Collision Time (ACT), which extends TTC to the 2D plane and has broad applicability. Moreover, several sub-indicators can be derived from ACT, including the Time of Evasive Action (TEA), which specifically considers evasive behavior. Kar et al. (2023) used ACT to assess the impact of speed differences on the risk of sideswipe collisions in mixed traffic. It is important to note that TTC-based SSMs primarily focus on how much time remains before the geometric centers of two vehicles converge in a certain direction, as depicted in state B of Figure 1(a). However, state A represents the actual crash moment. This paper highlights that in 2D situations, the TTC approach should not be directly applied to calculate proximity, as this may lead to optimistic estimates of collision times.

Existing 2D-SSMs, while applicable to 2D situations, essentially still employ a 1D-SSM unidirectional quantification framework, which can lead to inaccurate estimations of proximity to collision. We believe that a proper 2D-SSM should accurately represent the evasive difficulty of vehicle-pair in all directions. Specifically, for the scenario illustrated in Figure 1(b), both combined metrics like 2D-TTC and extended TTC methods such as ETTC would likely assess that Vehicles A and A' have the similar proximity to collision. However, it is evident that the actual risk faced by Vehicle A' is significantly lower than that of Vehicle A, as Vehicle A' has better maneuverability for evasive actions, including steering or combined lateral and longitudinal avoidance. Therefore, the core need for

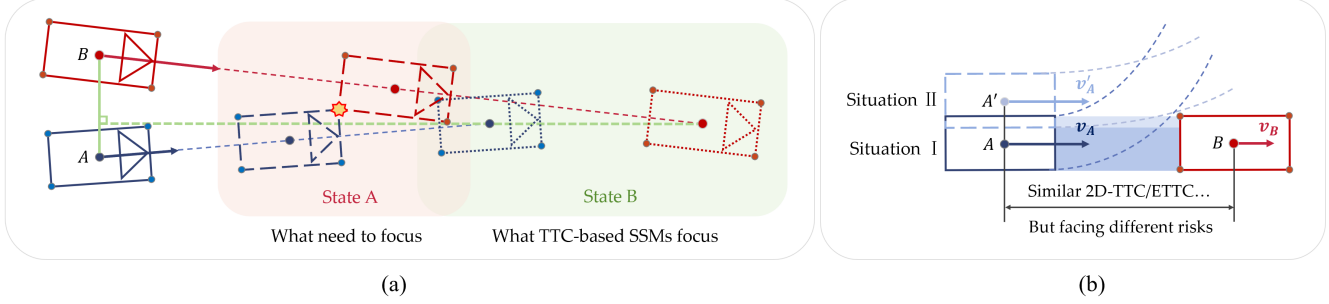


Figure 1: Diagram of the limitations of existing 2D-SSMs. (a) TTC-based SSMs focus on time to state B, which can lead to an optimistic estimation of vehicle risk; however, state A should be considered the situation with the highest risk. (b) Most existing 2D-SSMs still follow the calculation framework of 1D-SSMs; however, this unidirectional proximity measure is inadequate for accurately quantifying risk in 2D scenarios.

2D-SSMs is to incorporate both temporal proximity and the necessary evasive maneuvers across all directions while integrating the diverse driving states and conflict relationships into an interpretable risk assessment framework.

Validating SSMs using real datasets is crucial for assessing their effectiveness. However, some SSMs, although theoretically proposed, lack validation with real datasets (Huang et al., 2020). A fundamental requirement for proximal SSMs is the accurate assessment of vehicle conflict risks. Since conflict risks fundamentally depend on whether a collision occurs (Peesapati et al., 2018), a key validation approach is to test whether the SSM can identify non-collision conflicts and collision events using appropriate thresholds. Xie et al. (2019) proposed a method for validating SSMs by examining the correlation between detected conflicts and recorded accidents. Perez et al. (2017) used ROC curves to validate the classification performance of various SSMs for conflict and collision events.

2.2. Preconditions of SSMs

Traditional SSMs' preconditions often exhibit a preference for certain types of conflicts. For example, TTC has two preconditions: (i) both vehicles must be in the same longitudinal space, typically assessed by determining if the vehicles are in the same lane (Mahmud et al., 2017), or by checking the lateral overlap of the vehicle bodies (Charly & Mathew, 2019); (ii) the following vehicle's speed should be higher than the leading vehicle.

For 2D risk evaluation, the preconditions for SSMs should not exhibit a preference for specific conflict types. Hou et al. (2014) provided three collision detection methods, but these methods rely on simulation techniques, simulating the movement of two rectangles representing vehicles at each time step and detecting when these bodies overlap. Meeting real-time requirements poses a key challenge. Laureshyn et al. (2010) proposed a two-step classification approach based on path overlaps and collision courses, classifying the spatial and temporal relations between two vehicles. However, simplifying vehicle bodies to lines and points in calculations may result in undetected close-range conflicts. Ward et al. (2015) noted that directly calculating potential 2D vehicle conflicts is challenging. To address this, they propose a simplified method called "Looming", which assesses whether surrounding vehicles are approaching and pose a collision risk to the ego vehicle, serving as the precondition for ETTC. The Looming method sets multiple "test points" on each vehicle. If any "test points" directed at a vehicle simultaneously widens its observation angle to both sides, the vehicle is considered to be approaching (Ward et al., 2015). Looming has three potential issues: (i) If too few "test points" are set, smaller road users may go undetected (as shown in Figure 2(a-1)), while too many "test points" may waste computational resources; (ii) In tangential grazing situations with other vehicles, the observation angle on one side may not increase, leading to undetected conflicts, as shown in Figure 2(a-2); (iii) Vehicle rotation can significantly alter observation angles, increasing the risk of overlooking conflicts, as depicted in Figure 2(a-3). Venthuruthiyil & Chunchu (2022) suggested that potential conflicts between two vehicles may relate to two conditions: (i) both vehicles are on a collision course, and (ii) their closing-in rate is positive. They provided formalized judgment method for identifying potential conflicts in rear-end and lane changing scenarios. The preconditions for 2D-TTC are implicit in its calculation formula (Guo et al., 2023): if two vehicles continue on their current trajectories, they will collide horizontally or vertically in the future, causing their bodies to overlap. This method breaks down vehicle conflicts into horizontal and vertical dimensions, potentially failing in situations involving conflicts at certain angles or changing angles (Figure 2(b)). Inadequate preconditions may overlook some types of conflicts or even collisions, failing to quantify their risks. Additionally,

a collision probability-based conflict detection method can serve as a precondition for TTC (Beauchamp et al., 2022). This approach typically uses motion extrapolation hypotheses to derive the probability distribution of a vehicle’s future states, approximating collision probability through discrete summation (Saunier et al., 2007, 2010). However, its reliance on numerical simulation may challenge computational efficiency, particularly in large-scale real-time systems.

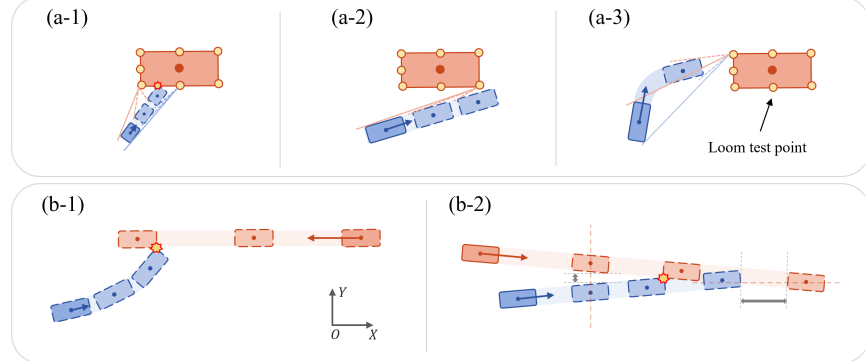


Figure 2: Inadequate preconditions of SSMs may overlook certain types of conflicts. (a) Conflicts undetectable by Looming. (b) Conflicts undetectable by 2D-TTC.

Ideal preconditions of SSMs should enable real-time detection and continuous updating of the “potential conflicts” set for each vehicle, further quantifying the risk levels of these potential conflicts. This paper contends that the conflict detection mechanisms of SSMs should minimize the possibility of missed detections. On the other hand, a certain level of false detections should be permissible, as even falsely detected scenarios can demonstrate low risk in the SSMs’ quantification outcomes.

3. Methodology

3.1. Overall framework and data format

We propose a framework for detecting and quantifying vehicle conflict risks, as shown in Figure 3. Initially, motion data from surrounding vehicles or all vehicles in the road environment are collected through on-board sensors or the vehicle-to-everything (V2X) communication. Then, the conflict detection model uses built-in conditions to filter out vehicle pairs with potential conflicts. Finally, the risk quantification model calculates real-time EI values for each vehicle-pair with potential conflicts, providing a quantitative assessment of the collision risk.

The motion data includes vehicle position, speed, heading angle, and vehicle size. For each instant, the state vector of vehicle A can be obtained as $\mathbf{S}_A = (x_A, y_A, v_A, \theta_A, l_A, w_A)^T$, where x_A and y_A represent the X and Y coordinates of the geometric center of vehicle A, v_A and θ_A represent the speed magnitude and speed direction angle, and l_A and w_A represent the length and width of the vehicle, respectively. Then, the position vector \mathbf{P}_A , velocity vector \mathbf{v}_A , and velocity direction vector $\boldsymbol{\theta}_A$ can be expressed as:

$$\begin{cases} \mathbf{P}_A = \overrightarrow{OA} = [x_A, y_A]^T \\ \mathbf{v}_A = [v_A \cos(\theta_A), v_A \sin(\theta_A)]^T \\ \boldsymbol{\theta}_A = [\cos(\theta_A), \sin(\theta_A)]^T = \frac{\mathbf{v}_A}{\|\mathbf{v}_A\|} \end{cases} \quad (1)$$

3.2. Conflict detection methods

Based on insights from previous research on conflict definitions (Laureshyn et al., 2010; Venthuruthiyil & Chunchu, 2022), we define potential conflicts by the following two qualitative conditions: (1) Overlapping travel spaces of two vehicles; (2) A trend of further contraction in the spatial gap between the vehicles. We emphasize that satisfying only one of these conditions does not constitute a potential conflict. In Figure 4(a), although the travel spaces of the two vehicles overlap, they are moving away from each other due to speed differences. In Figure 4(b), the vehicles are approaching each other, but their paths do not intersect, so this too is not classified as a

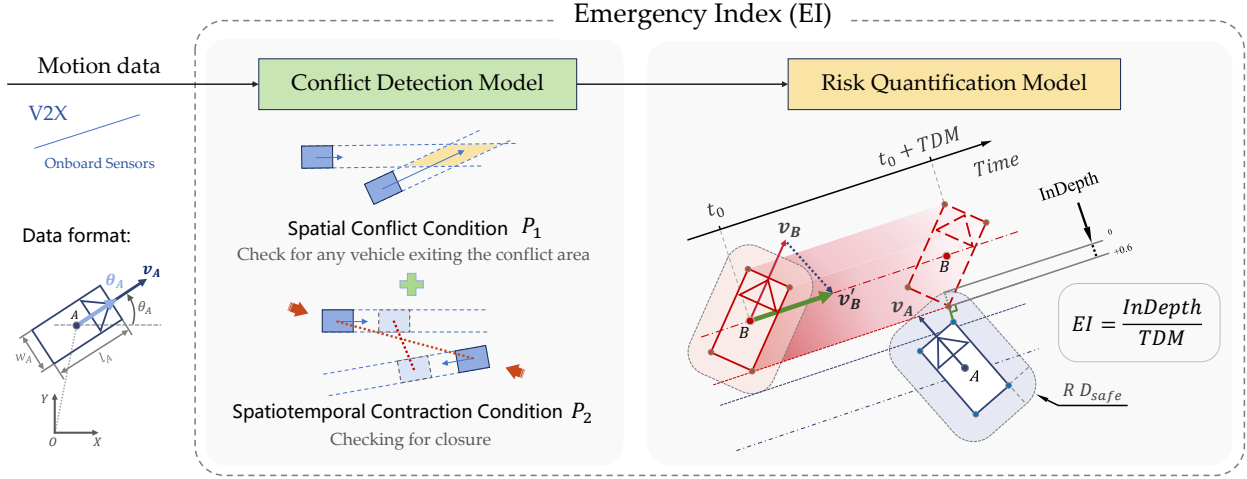


Figure 3: The framework of EI comprises two parts: the conflict detection model and the risk quantification model.

potential conflict. Only when both conditions are met does a potential conflict hold, as illustrated in Figure 4(c). However, qualitative conditions alone do not allow for objective and actionable judgments. The following section will demonstrate the process of transforming these two qualitative conditions into formalized criteria.

We define the existence of a potential conflict between vehicles as event Q , with two conditions P_i ($i = 1, 2$), where P_1 is the spatial conflict condition and P_2 is the spatiotemporal contraction condition. Each condition P_i is a necessary condition for event Q to hold, meaning that for each $i \in \{1, 2\}$, if Q holds, then P_i also holds. This is equivalent to stating that if $\neg P_i$ holds, then $\neg Q$ also holds.

$$\neg P_i \Rightarrow \neg Q \quad (2)$$

The sufficient and necessary condition for event Q to occur is that both criteria P_1 and P_2 are met. In other words, for each $i \in \{1, 2\}$:

$$Q \Leftrightarrow (P_1 \cap P_2) \quad (3)$$

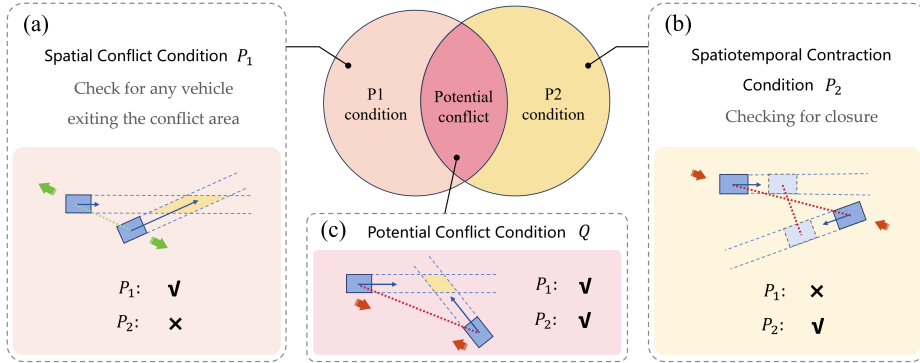


Figure 4: Conditions required for a potential conflict. (a) Spatial conflict condition P_1 . (b) Spatiotemporal contraction condition P_2 . (c) If both P_1 and P_2 are satisfied, then condition Q is satisfied, indicating the existence of a potential conflict.

3.2.1. Spatial conflict condition P_1

a. Problem definitions

In this paper, we use “strip” to describe the space currently and potentially occupied by a vehicle as it travels, which some studies refer to as the “driving corridor” (Hillenbrand et al., 2006). Under the constant velocity (CV) model, a vehicle’s strip can be described as: a 2D strip-shaped region within the driving space. As the vehicle moves forward, its rear end translates along the travel direction, sweeping out an area that is fixed at one end and extends indefinitely at the other, as shown in Figure 5(a). Vehicles A and B meet the spatial conflict condition P_1 if and only if strip_A and strip_B overlap in the 2D space.

$$P_1 = (\text{strip}_A \cap \text{strip}_B \neq \emptyset) \quad (4)$$

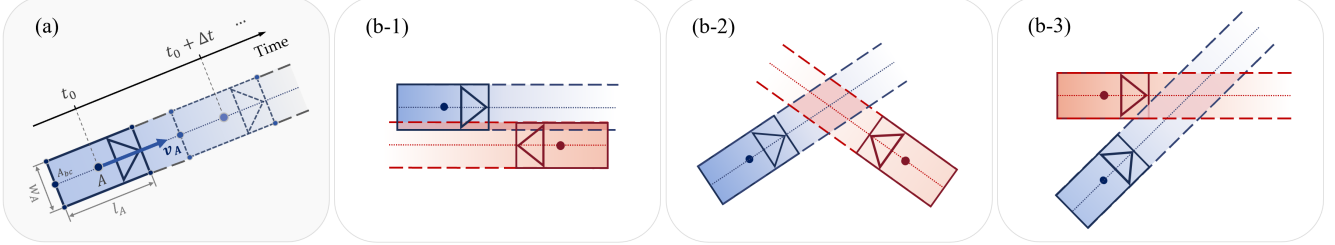


Figure 5: “Strip” represents the space currently and potentially occupied by a vehicle. (a) Diagram of the driving strip at t_0 . (b) Whether it is a parallel, angle, or sideswipe conflict, a common characteristic is the overlapping area between the strips of two vehicles.

Moreover, it is imperative to further translate the preceding descriptive condition into a mathematical condition. Initially, we determine the coordinates of the midpoint $P_{A,bc}$ along the rear segment of the vehicle, denoted as $P_{A,bc}$, for a specified orientation angle θ_A :

$$\mathbf{P}_{A,bc} = \mathbf{P}_A - \frac{l_A}{2}\boldsymbol{\theta}_A = \begin{pmatrix} x_A - \frac{l_A}{2} \cos(\theta_A) \\ y_A - \frac{l_A}{2} \sin(\theta_A) \end{pmatrix} \quad (5)$$

where l_A denotes the vehicle length. And the expression for the rear segment $Q_{A,bc}(k_A)$ is formulated as follows:

$$\mathbf{Q}_{A,bc}(k_A) = \mathbf{P}_{A,bc} + k_A \mathbf{d}_A, \quad k_A \in \left(-\frac{w_A}{2}, \frac{w_A}{2}\right) \quad (6)$$

The segment $Q_A(k_A)$ translates along direction $\boldsymbol{\theta}_A$, forming $\text{strip}_A(s_A, k_A)$. The formula is:

$$\text{strip}_A(s_A, k_A) = \mathbf{P}_{A,bc} + s_A \boldsymbol{\theta}_A + k_A \mathbf{d}_A, \quad s_A \in (0, s_{A,\max}), \quad k_A \in \left(-\frac{w_A}{2}, \frac{w_A}{2}\right) \quad (7)$$

where s_A is a scalar parameter, and $s_{A,\max}$ restricts the vehicle from driving out of the current road. For the condition P_1 wherein there exists an overlapping region between strip_A and strip_B , the descriptive condition can be transformed into a mathematically defined condition as follows:

$$P_1 = \left(\left\{ \mathbf{S}_A, \mathbf{S}_B \mid \begin{array}{l} \exists s_A \in (0, s_{A,\max}), k_A \in \left(-\frac{w_A}{2}, \frac{w_A}{2}\right), s_B \in (0, s_{B,\max}), k_B \in \left(-\frac{w_B}{2}, \frac{w_B}{2}\right) \\ \text{s.t. } \mathbf{P}_A + s_A \boldsymbol{\theta}_A + k_A \mathbf{d}_A = \mathbf{P}_B + s_B \boldsymbol{\theta}_B + k_B \mathbf{d}_B \end{array} \right\} \neq \emptyset \right) \quad (8)$$

Directly applying Eq.(8) would encounter computational difficulties. Consequently, this paper presents a geometry-based algorithm for efficiently solving P_1 . To ensure a rigorous derivation process, the spatial conflict condition P_1 is divided into non-parallel scenarios P_{1-1} and parallel scenarios P_{1-2} :

$$P_1 \equiv P_{1-1} \cup P_{1-2} \quad (9)$$

b. Spatial conflict condition in non-parallel scenarios P_{1-1}

For the non-parallel scenarios, this is considered as condition P_{1-1-1} :

$$P_{1-1-1} = (\{S_A, S_B \mid \theta_A \neq \pm \theta_B\} \neq \emptyset) \quad (10)$$

P_{1-1-1} refers to the situation where neither vehicle has completely exited the potential conflict area (PCA), i.e., if either vehicle leaves the PCA, it is identified that there is no conflict between the two vehicles, as shown in Figure 6(a). The PCA is a parallelogram region, denoted as parallelogram $C_1C_2C_3C_4$, with point C as the geometric centroid. P'_B is defined as the relative coordinates of vehicle B in the coordinate system of vehicle A:

$$\mathbf{d}'_B = \overrightarrow{AB} = \begin{bmatrix} x_B - x_A \\ y_B - y_A \end{bmatrix} \quad (11)$$

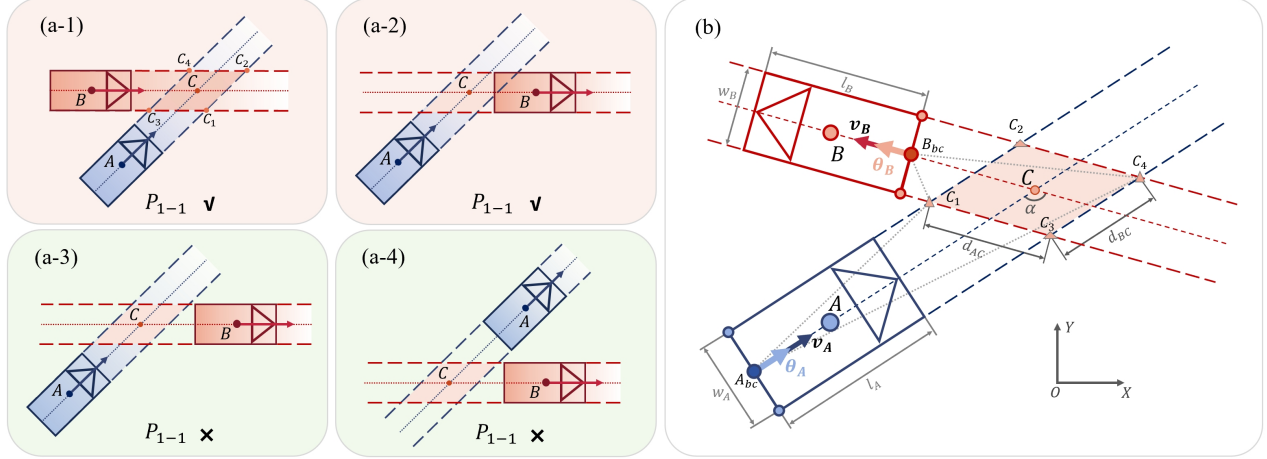


Figure 6: Spatial conflict condition considering vehicle dimensions in non-parallel scenarios. (a) Diagram illustrating whether P_{1-1} is established. (b) Diagram illustrating the determination and calculation of P_{1-1} .

According to geometric relationships, the coordinates of point C, P_C are as follows:

$$\mathbf{P}_C = \mathbf{P}_A + \overrightarrow{AC} = \mathbf{P}_A + t_A \boldsymbol{\theta}_A = \mathbf{P}_B + \overrightarrow{BC} = \mathbf{P}_B + t_B \boldsymbol{\theta}_B \quad (12)$$

where t_A and t_B are parameters of the space, $t_A, t_B \in (-\infty, \infty)$. Further, according to geometric relationships:

$$t_A \boldsymbol{\theta}_A = \mathbf{P}'_B + t_B \boldsymbol{\theta}_B \quad (13)$$

Both sides of the equation are simultaneously cross-multiplied by $\boldsymbol{\theta}_B$ on the right side. Since $\boldsymbol{\theta}_B \times \boldsymbol{\theta}_B = 0$, simplification yields:

$$\boldsymbol{\theta}_B \times t_A \boldsymbol{\theta}_A = \boldsymbol{\theta}_B \times \mathbf{P}'_B \quad (14)$$

Therefore:

$$t_A (\boldsymbol{\theta}_B \times \boldsymbol{\theta}_A) - \boldsymbol{\theta}_B \times \mathbf{P}'_B = 0 \quad (15)$$

As $\boldsymbol{\theta}_B$ is not parallel to $\boldsymbol{\theta}_A$, $\boldsymbol{\theta}_A \times \boldsymbol{\theta}_B \neq 0$:

$$t_A = \frac{\boldsymbol{\theta}_B \times \mathbf{P}'_B}{\boldsymbol{\theta}_B \times \boldsymbol{\theta}_A} \quad (16)$$

$$\mathbf{P}_C = \mathbf{P}_A + \left(\frac{\boldsymbol{\theta}_B \times \mathbf{P}'_B}{\boldsymbol{\theta}_B \times \boldsymbol{\theta}_A} \right) \cdot \boldsymbol{\theta}_A \quad (17)$$

The angle between the velocity directions $\boldsymbol{\theta}_A$ and $\boldsymbol{\theta}_B$ is defined as α :

$$\alpha = \arccos(\boldsymbol{\theta}_A \cdot \boldsymbol{\theta}_B) \quad (18)$$

The lengths of the sides d_{AC} and d_{BC} of the PCA parallelogram $C_1C_2C_3C_4$ can be determined as:

$$\begin{cases} d_{AC} = \frac{1}{\sin \alpha} \cdot w_A = \frac{w_A}{\sqrt{1-(\theta_A \cdot \theta_B)^2}} \\ d_{BC} = \frac{1}{\sin \alpha} \cdot w_B = \frac{w_B}{\sqrt{1-(\theta_A \cdot \theta_B)^2}} \end{cases} \quad (19)$$

Consequently, the coordinates of each vertex \mathbf{P}_{C_i} of the PCA parallelogram can be determined as:

$$\mathbf{P}_{C_i} = \mathbf{P}_C + (-1)^i \frac{d_{BC}}{2} \theta_A + (-1)^{\lfloor (i-1)/2 \rfloor} \frac{d_{AC}}{2} \theta_B, \quad i \in \{1, 2, 3, 4\} \quad (20)$$

The expressions for the vectors $\overrightarrow{A_{bc}C_i}$ and $\overrightarrow{B_{bc}C_i}$ from the midpoints A_{bc} and B_{bc} of the vehicle's rear segments to each vertex C_i of the parallelogram are as follows:

$$\begin{cases} \overrightarrow{A_{bc}C_i} = \mathbf{P}_{C_i} - \mathbf{P}_{A,bc}, & i \in \{1, 2, 3, 4\} \\ \overrightarrow{B_{bc}C_i} = \mathbf{P}_{C_i} - \mathbf{P}_{B,bc}, & i \in \{1, 2, 3, 4\} \end{cases} \quad (21)$$

A vehicle completely exits the PCA if and only if its rear segment entirely leaves the PCA. As shown in Figure 6(b), for vehicle B, this condition is satisfied if, for all $i \in \{1, 2, 3, 4\}$, the angle between θ_B and $\overrightarrow{B_bC_i}$ is greater than 90° , i.e., $\theta_B \cdot \overrightarrow{B_bC_i} < 0$. Meanwhile, the condition for vehicle A not having departed from the PCA is:

$$\exists i \in \{1, 2, 3, 4\}, \text{s.t. } \theta_A \cdot \overrightarrow{A_{bc}C_i} > 0 \quad (22)$$

In summary, the necessary and sufficient condition for P_{1-1} is that neither vehicle A nor vehicle B has departed from the PCA. The mathematical expression for the spatial conflict condition in non-parallel scenarios is:

$$P_{1-1-2} = \left(\{\mathbf{S}_A, \mathbf{S}_B \mid \exists i, j \in \{1, 2, 3, 4\}, \text{s.t. } (\theta_A \cdot \overrightarrow{A_{bc}C_i}) > 0 \cap (\theta_B \cdot \overrightarrow{B_{bc}C_j}) > 0 \} \neq \emptyset \right) \quad (23)$$

$$P_{1-1} \equiv P_{1-1-1} \cap P_{1-1-2} \quad (24)$$

c. Spatial conflict condition in parallel scenarios P_{1-2}

For the scenarios where the velocity directions of both vehicles are parallel, i.e., $\theta_A = \pm \theta_B$, the discussion essentially revolves around whether $strip_A$ and $strip_B$ overlap. However, unlike the non-parallel case, the point C cannot be detected. The determination condition P_{1-2} can be divided into three parts: P_{1-2-1} , P_{1-2-2} , and P_{1-2-3} , as shown in Figure 7.

P_{1-2-1} represents the parallel condition. P_{1-2-2} concerns the minimum longitudinal distance between the two vehicles. P_{1-2-3} concerns the minimum lateral distance between the two vehicles. The mathematical representation of the three conditions is as follows:

$$P_{1-2-1} = (\{\mathbf{S}_A, \mathbf{S}_B \mid \theta_A = \pm \theta_B\} \neq \emptyset) \quad (25)$$

$$\left\{ \begin{array}{l} P_{1-2-2} = \left(\{\mathbf{S}_A, \mathbf{S}_B \mid (\overrightarrow{AB} \cdot \theta_A \geq 0) \cup (\overrightarrow{BA} \cdot \theta_B \geq 0) \cup (D_l \leq D_{\min})\} \neq \emptyset \right) \\ D_l = \|\overrightarrow{AB} \times \theta_A^\perp\| = \|\overrightarrow{BA} \times \theta_B^\perp\| \\ D_{l,\min} = \frac{l_A + l_B}{2} \end{array} \right. \quad (26)$$

$$\left\{ \begin{array}{l} P_{1-2-3} = (\{\mathbf{S}_A, \mathbf{S}_B \mid (D_w \leq D_{w,\min})\} \neq \emptyset) \\ D_w = \|\overrightarrow{AB} \times \theta_A\| = \|\overrightarrow{BA} \times \theta_B\| \\ D_{w,\min} = \frac{w_A + w_B}{2} \end{array} \right. \quad (27)$$

$$P_{1-2} \equiv P_{1-2-1} \cap P_{1-2-2} \cap P_{1-2-3} \quad (28)$$

Although perfectly parallel scenarios are rare, condition P_{1-2} can be applied to nearly parallel situations, such as ideal car-following.

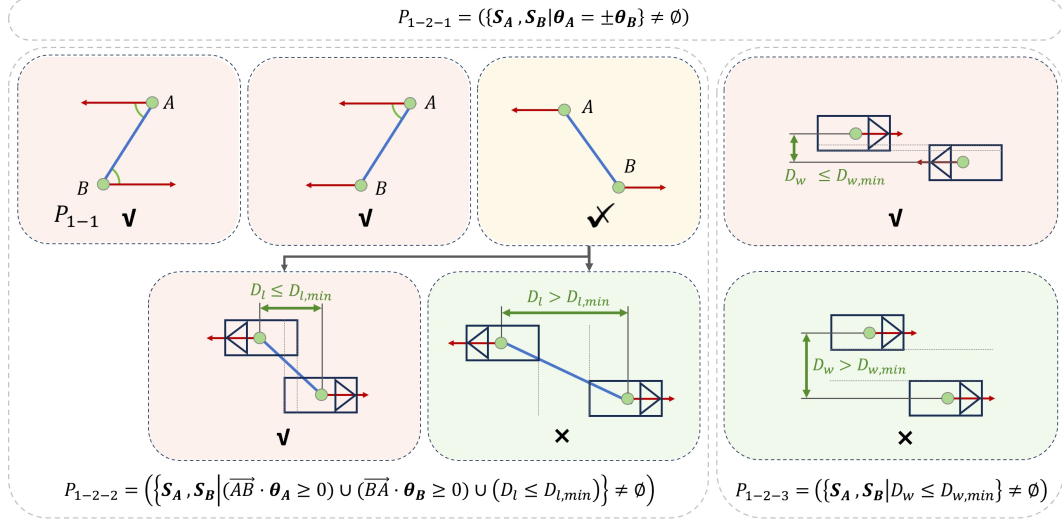


Figure 7: Spatial conflict condition considering vehicle dimensions in non-parallel scenarios.

3.2.2. Spatiotemporal contraction condition P_2

As described above, another necessary condition for potential conflict between vehicles is the tendency for the spatial gap between the vehicles to contract. In vehicle A's coordinate system $X'AY'$, the relative coordinate vector of vehicle B is denoted as $\mathbf{P}'_B = \overrightarrow{AB} = (x_B - x_A, y_B - y_A)^T = (x'_B, y'_B)^T$, and its relative velocity vector is v'_B :

$$\mathbf{v}'_B = \mathbf{v}_B - \mathbf{v}_A = \begin{bmatrix} v_B \cos(\theta_B) - v_A \cos(\theta_A) \\ v_B \sin(\theta_B) - v_A \sin(\theta_A) \end{bmatrix} \quad (29)$$

The radial component $v'_{B,r}$ and tangential component $v'_{B,t}$ of the relative velocity of vehicle B are:

$$\begin{cases} v'_{B,r} = -\frac{\mathbf{P}'_B}{\|\mathbf{P}'_B\|} \cdot \mathbf{v}'_B \\ v'_{B,t} = -\frac{\mathbf{P}'_B}{\|\mathbf{P}'_B\|} \cdot \mathbf{v}'_B^\perp \end{cases} \quad (30)$$

The spatiotemporal contraction condition P_2 , as illustrated in Figure 8, can be mathematically expressed as follows:

$$P_2 = (\{\mathbf{S}_A, \mathbf{S}_B \mid (\mathbf{P}'_B \cdot \mathbf{v}'_B < 0)\} \neq \emptyset) \quad (31)$$

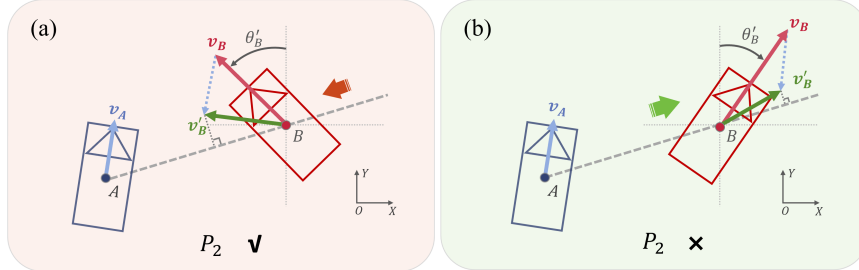


Figure 8: Spatiotemporal contraction condition P_2 . (a) P_2 satisfied. (b) P_2 not satisfied.

The following is the proof of P_2 . For the initial time t_0 , the relative distance between the vehicles is:

$$D(t_0) = \|\mathbf{P}'_B(t_0)\| = \sqrt{x'^2_B + y'^2_B} \quad (32)$$

For the time $t_0 + \Delta t$, the relative distance between the vehicles is:

$$D(t_0 + \Delta t) = \|\mathbf{P}'_B(t_0 + \Delta t)\| = \sqrt{\left(D(t_0) - \Delta t v'_{B,r}\right)^2 + \left(\Delta t v'_{B,t}\right)^2} \quad (33)$$

Taking the derivative of $D(t_0 + \Delta t)$ with respect to time Δt :

$$\frac{dD}{dt} = \frac{\Delta t \left[(v'_{B,t})^2 + (v'_{B,r})^2 \right] - 2v'_{B,r} D(t_0)}{2\sqrt{\left(\Delta t v'_{B,t}\right)^2 + (D(t_0) - \Delta t v'_{B,r})^2}} \quad (34)$$

$$\lim_{\Delta t \rightarrow 0^+} \frac{dD}{dt} = \frac{-v'_{B,r} D(t_0)}{D(t_0)} = -v'_{B,r} \quad (35)$$

Therefore, there exists $\varepsilon > 0$ such that for all $\Delta t \in (0, \varepsilon)$, we have $\frac{dD}{dt} < 0$. If Δt is controlled within a sufficiently small range, the necessary and sufficient condition for the distance between the two vehicles to decrease is $v'_{B,r} > 0$, while the necessary and sufficient condition for $v'_{B,r} > 0$ is $\mathbf{P}'_B \cdot \mathbf{v}'_B < 0$, which satisfies the spatiotemporal contraction condition P_2 . Notably, we assume that even if two vehicles are very close, they are not in danger as long as they are moving away from each other. However, if they start to approach each other, our method can quickly detect potential conflicts.

3.3. Risk quantification model: Emergency Index (EI)

For each vehicle-pair detected by the CDM, risk quantification is continued. We extract the velocity direction $\boldsymbol{\theta}'_B$ of vehicle B relative to vehicle A:

$$\boldsymbol{\theta}'_B = \frac{\mathbf{v}'_B}{\|\mathbf{v}'_B\|} \quad (36)$$

Starting from the initial time t_0 , we define the distance between the centroids of the two vehicles at time t as $D(t)$. Define the Time-to-Depth-Maximum (TDM) as the time from the current moment until the shortest distance is reached between the vehicles' bodies. The minimum distance between the centroids is $D(t_0 + TDM)$:

$$D(t_0 + TDM) = \|\mathbf{P}'_B \times \boldsymbol{\theta}'_B\| \quad (37)$$

Considering the vehicle dimensions, we continue to derive the projected Minimum Future Distance (MFD) between the vehicles based on the current trajectory. First, we calculate the vectors from the vehicle geometric center point to each vertex of the vehicle body rectangle, denoted as $\overrightarrow{AA_i}$ and $\overrightarrow{BB_j}$.

$$\begin{cases} \overrightarrow{AA_i} = (-1)^{\lfloor \frac{i-1}{2} \rfloor} \frac{l_A}{2} \boldsymbol{\theta}_A + (-1)^i \frac{w_A}{2} \boldsymbol{\theta}_A^\perp, & i \in \{1, 2, 3, 4\} \\ \overrightarrow{BB_j} = (-1)^{\lfloor \frac{j-1}{2} \rfloor} \frac{l_B}{2} \boldsymbol{\theta}_B + (-1)^j \frac{w_B}{2} \boldsymbol{\theta}_B^\perp, & j \in \{1, 2, 3, 4\} \end{cases} \quad (38)$$

The $\boldsymbol{\theta}_A^\perp$ follows the right-hand rule, which is obtained by rotating $\boldsymbol{\theta}_A$ clockwise by 90° . Considering the vehicle dimensions, the MFD should at least consider the surplus of d_A and d_B , otherwise a collision may still occur. The geometric meaning of d_A is the maximum value of the projection of the vector from the vehicle center point to the vehicle vertex, $\overrightarrow{AA_i}$, in the direction perpendicular to the relative velocity, and similarly for d_B .

$$\begin{cases} d_A = \|\overrightarrow{AA_i} \times \boldsymbol{\theta}'_B\|, & i = \arg \max_{i \in \{1, 2, 3, 4\}} \|\overrightarrow{AA_i} \times \boldsymbol{\theta}'_B\| \\ d_B = \|\overrightarrow{BB_j} \times \boldsymbol{\theta}'_B\|, & j = \arg \max_{j \in \{1, 2, 3, 4\}} \|\overrightarrow{BB_j} \times \boldsymbol{\theta}'_B\| \end{cases} \quad (39)$$

Specifically, if there are two i that both maximize the expression, choose the i corresponding to the A_i that is positioned earlier in the $\boldsymbol{\theta}'_B$ direction. For j , the latter one is selected. (i is 2 and j is 4 in Figure 9(c))

Thus, we can calculate the MFD between vehicles:

$$MFD = D(t_0 + TDM) - (d_A + d_B) \quad (40)$$

After the period of TDM, when the corner points of the vehicles reach the shortest distance the original $\overrightarrow{A_iB_j}$ becomes $\overrightarrow{A_iB_j} + TDM \times \mathbf{v}'_B$. Since the distance is the minimum, $(\overrightarrow{A_iB_j} + TDM \times \mathbf{v}'_B) \perp \theta'_B$. Therefore, the formula for TDM is as follows:

$$TDM = \frac{\overrightarrow{B_jA_i} \cdot \theta'_B}{\|\mathbf{v}'_B\|} \quad (41)$$

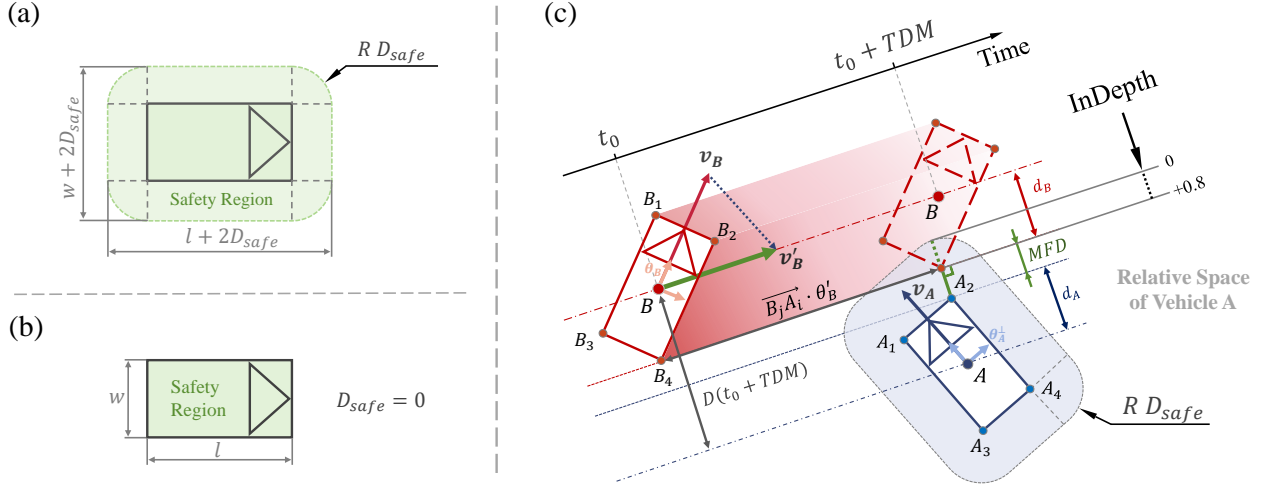


Figure 9: The risk quantification model considers InDepth and TDM. (a) Diagram of the safety region. (b) Diagram of the safety region when D_{safe} is set to 0. (c) Diagram illustrating TDM, MFD, and InDepth in a two-vehicle conflict.

The safety region is defined as the area a vehicle needs to keep clear of other vehicles to ensure its own safety. The safety region is a rounded rectangle that encompasses the vehicle's body rectangle, with a corner radius of D_{safe} , as shown in Figure 9(a). When $MFD \geq D_{safe}$, it indicates that the current risk is acceptable. When $MFD < D_{safe}$, it indicates that the current risk is unacceptable, necessitating an evasive maneuver. In a connected environment, when any two vehicles interact, the determination method for D_{safe} is proposed as shown in Eq.(42).

$$D_{safe} = \max\{D_{safe,A}, D_{safe,B}\} \quad (42)$$

where $D_{safe,A}$ and $D_{safe,B}$ are the acceptable minimum clearance distances for each vehicle. The setting of D_{safe} contains subjective elements regarding risk sensitivity, which may be related to driving style and vehicle speed. It is proposed that a civilized driving behavior takes into account the risk sensitivity of both the ego vehicle and surrounding vehicles. Therefore, when considering evasive maneuvers, the ego vehicle should consider the maximum D_{safe} between itself and surrounding vehicles. For instance, in a conflict between a high-speed vehicle and a very low-speed vehicle, priority should be given to the larger D_{safe} value corresponding to the high-speed vehicle. In the case represented in Figure 9(c), D_{safe} is chosen as $\max\{D_{safe,A}, D_{safe,B}\} = D_{safe,A}$. The specific D_{safe} setting method can refer to previous literature (Yao et al., 2013; Wang et al., 2015; Jiao et al., 2023) and is not the focus of this paper.

We propose the concept of Interaction Depth (InDepth) to measure the maximum depth two vehicles are projected to intrude into each other's safety region, as shown in Figure 9(c). The calculation formula is as follows:

$$InDepth = D_{safe} - MFD \quad (43)$$

The time until reaching the peak risk moment is known as TDM in Eq.(41). For vehicles in a near-crash scenario, they must execute evasive maneuvers within the TDM period to mitigate the danger, with InDepth representing

the necessary adjustments between the two vehicles to avoid a collision. Thus, we propose a 2D-SSM, named the Emergency Index (EI), defined as the ratio of InDepth to TDM:

$$EI = \frac{InDepth}{TDM} \quad (44)$$

It can be observed that $EI > 0$ indicates the need for vehicles to take collision avoidance measures, whereas $EI \leq 0$ suggests that no change in motion is necessary for avoidance. As the remaining time decreases or the required change increases, the value of EI increases, indicating a positive correlation between the EI value and the current risk of conflict for the vehicles. The physical significance of EI lies in the rate of change in InDepth required for evasive actions. In other words, EI represents the intensity of evasive maneuvers needed by the two vehicles to avoid a collision.

For events that require evasive actions with limited remaining response time, we define these events as critical conflicts. By setting an appropriate TDM threshold, i.e., TDM^* , critical conflicts can be defined as follows: if and only if, at any given moment t , the vehicle pair satisfies: (1) $TDM(t) \leq TDM^*$ and (2) $InDepth(t) \geq 0$. The value of TDM^* can refer to thresholds of time-based SSMs such as TTC, for example, setting $TDM^* = 1.5$ s, though further validation is needed. In more hazardous situations, before TDM reaches zero, it is essential to ensure that $InDepth \leq D_{safe}$; otherwise, a collision will occur. Thus, a crash event can be defined as follows: if and only if, at any given moment t , the vehicle pair satisfies: (1) $TDM(t) \rightarrow 0$ and (2) $InDepth(t) \geq D_{safe}$. Consequently, EI can represent collision avoidance risk across various forms of conflict within a unified interaction risk level. When combined with its precondition, CDM, EI enables the quantitative classification of non-conflict, potential conflict, critical conflict, and crash, as shown in Table 1.

Table 1: The EI framework for judging potential conflict, critical conflict, and crash event

	Non-Conflict	Potential Conflict	Critical Conflict	Crash
$Q \Leftrightarrow (P_1 \cap P_2)$	×	✓	✓	✓
TDM (s)	-	-	$\leq TDM^*$	$\rightarrow 0$
InDepth (m)	-	-	≥ 0	$\geq D_{safe}$
EI (m/s)	-	-	≥ 0	$\rightarrow +\infty$

The only hyper-parameter in the EI framework is D_{safe} . Essentially, the D_{safe} setting provides a consideration for safety redundancy. When D_{safe} is set to zero, EI measures the baseline difficulty of collision avoidance between two vehicles without any safety margin. At this setting, the safety region is equivalent to the vehicle's body dimensions, as depicted in Figure 9(b). In the subsequent analysis and applications, we set D_{safe} to zero to test the applicability and validity of EI's core framework without incorporating a safety redundancy design.

4. Performance evaluation of EI

In this section, we first verify the effectiveness of the CDM in conflict detection through typical collision cases. Next, we conduct driving simulator experiments in four typical near-crash scenarios to validate EI's efficacy in risk quantification. After that, we analyze the impact of evasive maneuvers on EI through simulations. Finally, we validate the binary classification performance of EI for crash and conflict events using a large amount of real road and crash data.

4.1. Performance evaluation of CDM

To validate the effectiveness of CDM, we compare its detection results for typical collision cases with those of other methods, including the Looming method and 2D-TTC preconditions. The setup for each comparison method is as follows: In the Looming method, seven loom test points are set for each vehicle. Since Looming involves the concepts of an active and a passive vehicle, we consider a conflict to exist if any vehicle identifies a conflict with another. For consistency, we adjust the calculation reference point of 2D-TTC from the midpoint of the front bumper to the geometric center of the vehicle body. For probability-based methods, we adopt the collision

probability computation framework proposed by Saunier et al. (2010). Since potential conflict detection requires a trigger threshold, we set the collision probability threshold at 0.01 to signal a potential conflict.

Detection case 1 involves a crash scenario at an intersection between a left-turning vehicle and a straight-moving vehicle, as shown in Figure 10. It is assumed that the collision occurs at $t = 0$ s. CDM detects a potential vehicle conflict at $t = -1.64$ s and continuously tracks it until the moment of the potential collision. The Looming method underperforms, only detecting potential conflict between $t = -0.64$ s and $t = -0.11$ s. The 2D-TTC preconditions failed throughout the process, with no conflicts detected. The probability method detects a potential conflict at $t = -2.67$ s, but fails 0.09 s before the collision. This failure may occur because, when the vehicles are in close proximity, extrapolating their future positions based on current states can lead to nearly non-overlapping of position distributions, resulting in no conflict detection.

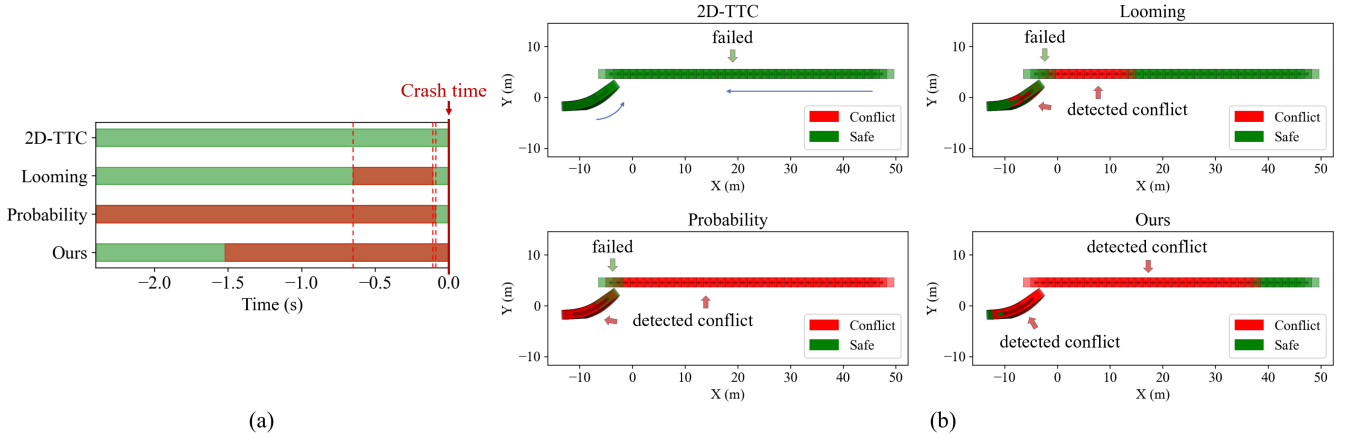


Figure 10: Detection case 1: A collision event between a left-turning vehicle and a straight-moving vehicle at an intersection. (a) The performance of four conflict detection methods, with red bars indicating potential conflict detection and green bars indicating no conflict detected. (b) Scenario diagram of conflict detection results, where the red vehicle positions represent detected potential conflicts, and the green vehicle positions represent states with no potential conflict detected.

Detection case 2 involves a low-speed leading vehicle merging and causing a sideswipe collision with the following vehicle, as shown in Figure 11. CDM and probability method demonstrate good conflict detection performance. However, both the 2D-TTC preconditions and Looming experience missed detections during the merging process of the lead vehicle.

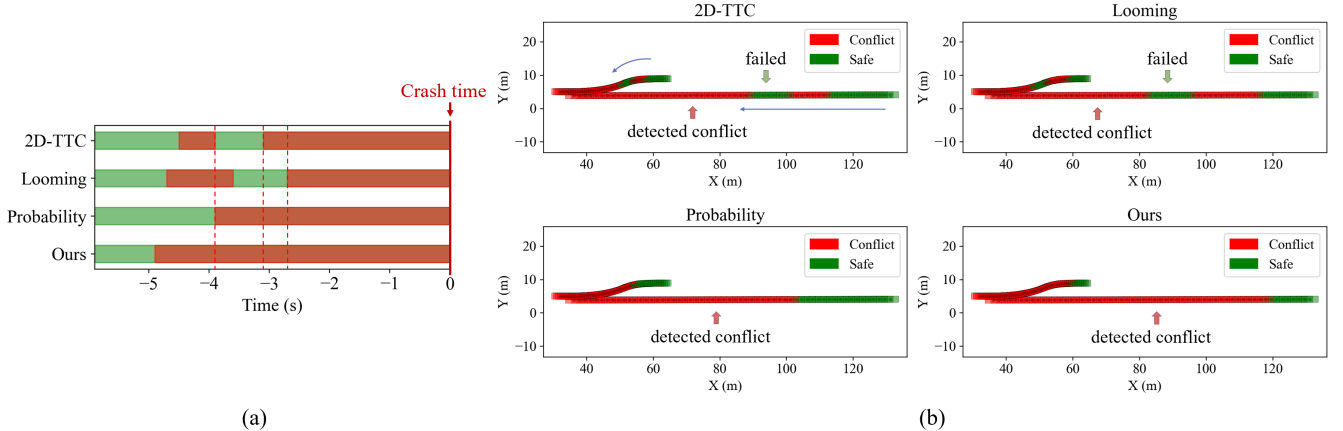


Figure 11: Detection case 2: A low-speed lead vehicle merging and causing a sideswipe collision with the following vehicle. (a) The performance of four conflict detection methods. (b) Scenario diagram of conflict detection results.

Table 2 summarizes the average per-frame computation time for the four conflict detection methods in the

two cases. The probability method exceeds 10 ms per frame in single-vehicle cases, presenting computational challenges in multi-vehicle scenarios. In contrast, SSM preconditions based on analytical methods offer good real-time performance, making them suitable for large-scale real-time road safety monitoring.

Table 2: Average computation time per frame for two potential conflict detected cases

Case	2D-TTC	Looming	Probability	CDM (Ours)
Case 1	0.082 ms	0.159 ms	10.679 ms	0.155 ms
Case 2	0.068 ms	0.152 ms	13.754 ms	0.168 ms

Overall, the experimental results indicate that CDM has the advantages of higher stability and lower missed detection rate compared to previously SSM preconditions. Additionally, it offers better real-time performance than probability-based methods.

4.2. Case study of driving simulator

Current research categorizes vehicle conflicts into four types: rear-end, sideswipe, angle, and head-on (Feng et al., 2023). This paper conducts simulator experiments for these four types of conflicts to validate the proposed method's real-time performance and effectiveness. The simulator reproduces various hazardous scenarios, capturing actual evasive maneuvers at a high sampling frequency of 100Hz for detailed risk indicator analysis. The experiments use SCANeR software and a cabin driving simulator, controlling all agents except the ego vehicle. The simulator includes a driving cabin and motion platform with real operational elements like a steering wheel, pedals, and dashboards(see Figure 12). Real-time views of the vehicle's surroundings are displayed, and vibrations and collision feedback are provided. All data are managed by a cloud server, with SCANeR's video review system allowing frame-by-frame analysis of past events.

As comparative SSMs, this paper uses the commonly employed TTC and TAdv, and utilizes ACT and 2D-TTC as representatives of 2D-SSMs.

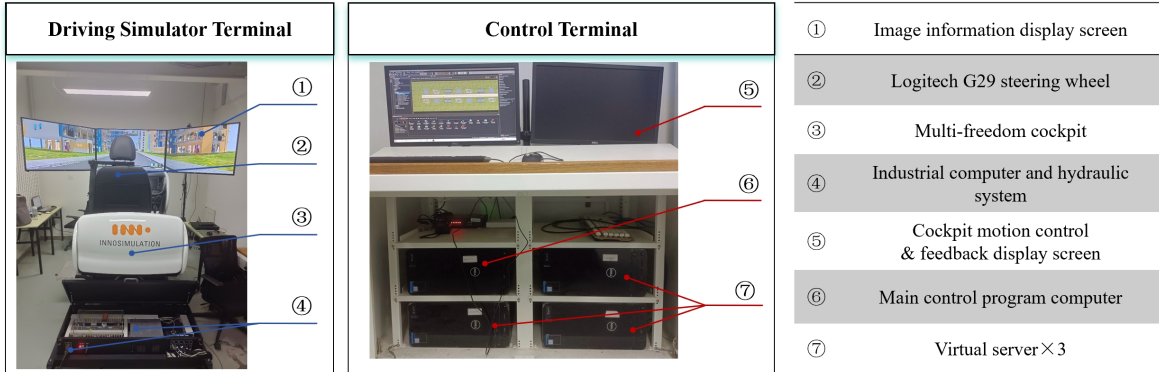


Figure 12: Driving simulator platform.

Scenario1: Rear-end. A near-miss rear-end case, as shown in Figure 13, involves two vehicles in the same lane. The ego vehicle (following vehicle) is operated by a human driver through a driving simulator, and the preceding vehicle (environment vehicle) is controlled by an Automatic Emergency Braking (AEB) system configured in the simulation environment. According to Table 3, the sequence is as follows: At $t = 9.33$ s, the preceding vehicle triggers emergency braking. At $t = 10.06$ s, the driver presses the brake pedal. At $t = 10.45$ s, the speed difference between vehicles peaks at 15.71 m/s. At $t = 11.04$ s, the deceleration of the ego vehicle reaches its maximum. The moments when EI peaks and ACT reaches its minimum are closely timed, occurring at $t = 11.32$ s and $t = 11.33$ s, respectively. The peak EI is 1.44 m/s, and the minimum ACT is 0.98 s. The minimum values of TTC and TAdv appear at $t = 12.07$ s and $t = 12.08$ s, respectively, with values of 0.31 s and 0.32 s. At $t = 12.43$ s, the ego vehicle stops. Neither condition P_1 nor P_2 is met, indicating no conflict. Overall, all indicators show similar trends over

time. EI and ACT peak approximately only 0.29 s after the ego vehicle's deceleration reaches its maximum. This implies a closer association of EI and ACT with the vehicle's evasive maneuvers. (Note: Here, the calculations for TTC and 2D-TTC are identical and thus are not differentiated)

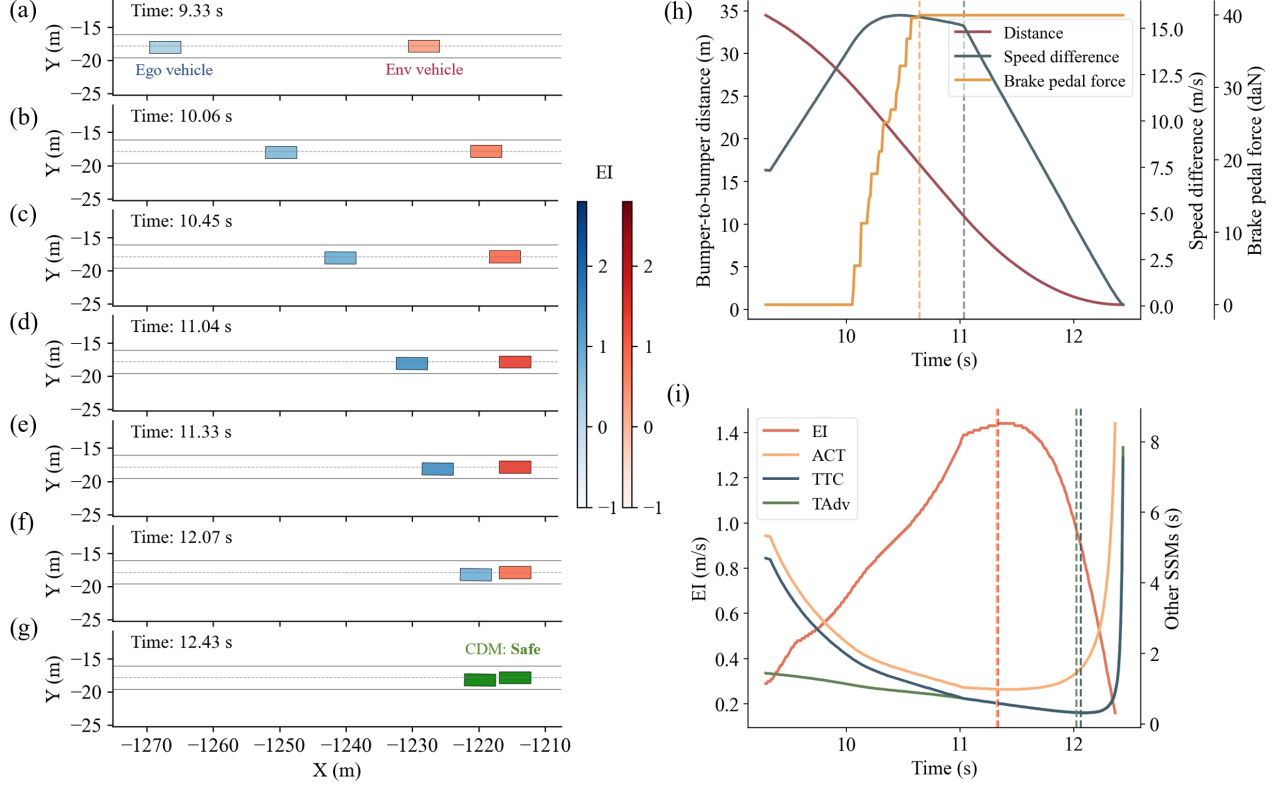


Figure 13: Scenario 1: Rear-end conflict. The preceding vehicle initiates emergency braking, and the ego vehicle engages braking to avoid a collision. (a)-(g) Visualizations of the scene at different moments. (h) Profiles of the bumper-to-bumper distance, speed difference, and the ego vehicle's brake pedal force over time. (i) Profiles of EI, ACT, TTC and TAdv over time.

Table 3: SSMs over time in scenario 1

Time (s)	P_1	P_2	EI (m/s)	ACT (s)	TTC (s)	TAdv (s)
9.33	✓	✓	0.30	5.31	4.66	1.43
10.06	✓	✓	0.72	2.16	1.83	1.10
10.45	✓	✓	0.94	1.58	1.28	0.94
11.04	✓	✓	1.39	1.03	0.72	0.72
11.33	✓	✓	1.44	0.98	0.58	0.58
12.07	✓	✓	0.88	1.61	0.31	0.32
≥ 12.43	✗	✗	—	—	—	—

Scenario 2: Sideswipe. A high-risk sideswipe case, as shown in Figure 14, involves a cut-in vehicle (ego vehicle) controlled by a human driver using the driving simulator platform, and a following vehicle (environment vehicle) controlled by the intelligent driver model (IDM)(Kesting et al., 2010). Referring to Table 4, the description is as follows: At $t = 4.18$ s, condition P_1 is not met, and the situation is detected as non-conflict. At $t = 4.6$ s, the ego vehicle initiates a lateral movement to the right, signaling a lane change, and at this moment P_1 is satisfied, indicating the presence of a conflict. At $t = 5.09$ s, ACT reaches its minimum value of 2.53 s. By $t = 5.19$ s, EI peaks at 1.09 m/s, TAdv drops to a minimum of 0.01 s, and ACT remains at 2.53 s, with the ego vehicle's lateral speed reaching -0.68 m/s. At $t = 5.28$ s, both 2D-TTC and TTC achieve their minimum values of 1.9 s. At $t = 6.54$ s, the vehicles reach equal speeds, and condition P_2 is not met. Overall, the extreme values of the five SSMs are concentrated within the time interval from 5.09 s to 5.28 s, showing consistency.

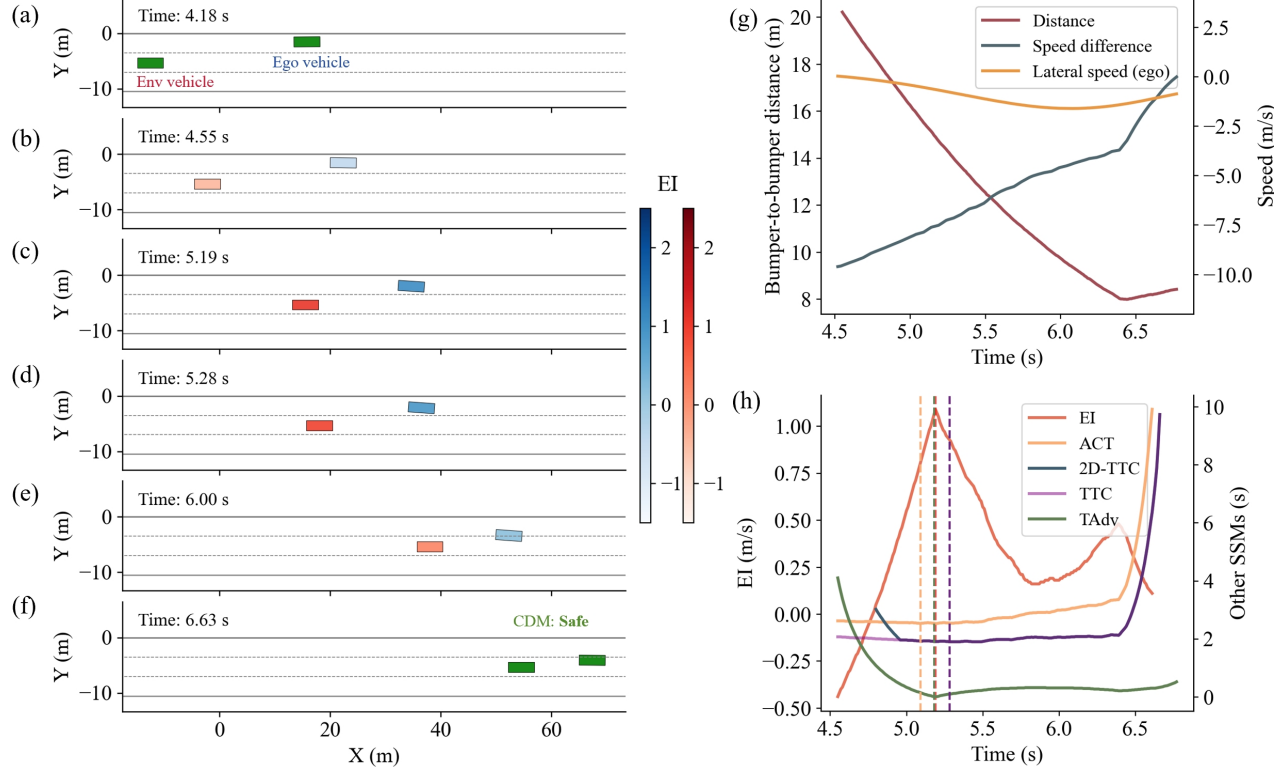


Figure 14: Scenario 2: Sideswipe conflict. In a highway scenario, the ego vehicle merges from the left to the middle lane, risking a conflict with a faster vehicle in the middle lane. The two vehicles reach equal speeds within two seconds. (a)-(f) Visualizations of the scene at different moments. (g) Profiles of the bumper-to-bumper distance, speed difference, and the ego vehicle’s lateral speed over time. (h) Profiles of EI, ACT, 2D-TTC, TTC and TAdv over time.

Table 4: SSMs over time in scenario 2

Time (s)	P_1	P_2	EI (m/s)	ACT (s)	2D-TTC (s)	TTC (s)	TAdv (s)
≤ 4.54	×	✓	—	—	—	—	—
4.55	✓	✓	-0.44	2.62	—	2.07	4.10
5.19	✓	✓	1.09	2.53	1.91	1.91	0.01
5.28	✓	✓	0.93	2.55	1.90	1.90	0.09
6.00	✓	✓	0.18	2.99	2.06	2.06	0.31
≥ 6.54	✓	✗	—	—	—	—	—

Scenario 3: Angle. An angle conflict at an intersection, as shown in Figure 15. The ego vehicle in the bottom right is human-driven, and the environment vehicle in the upper left travels straight at a constant speed of 16.67 m/s. The sequence of events, as outlined in Table 5, is as follows: At $t = 6.29$ s, the InDepth becomes positive. The driver applies the brakes at $t = 7.15$ s. At $t = 7.19$ s, TAdv reaches its minimum value of 0.08 s. At $t = 7.22$ s, the speed of the ego vehicle peaks at 6.91 m/s, then begins to decrease. At $t = 7.25$ s, EI reaches its maximum value; at this time, the speed of the ego vehicle is 6.89 m/s, EI is 2.14 m/s, ACT is 1.76 s, and both TTC and 2D-TTC are 1.57 s, with TAdv still at 0.08 s. At $t = 7.34$ s, 2D-TTC reaches its minimum value of 1.52 s. At $t = 8.59$ s, ACT reaches its minimum value of 0.84 s, with TTC at 0.22 s. Overall, EI, TAdv, and 2D-TTC effectively reflect the impact of the driver’s evasive actions on vehicle risk in this case. Specifically, before the driver’s evasive actions, EI continuously increases until it reaches a peak. After the driver’s evasive actions, EI decreases.

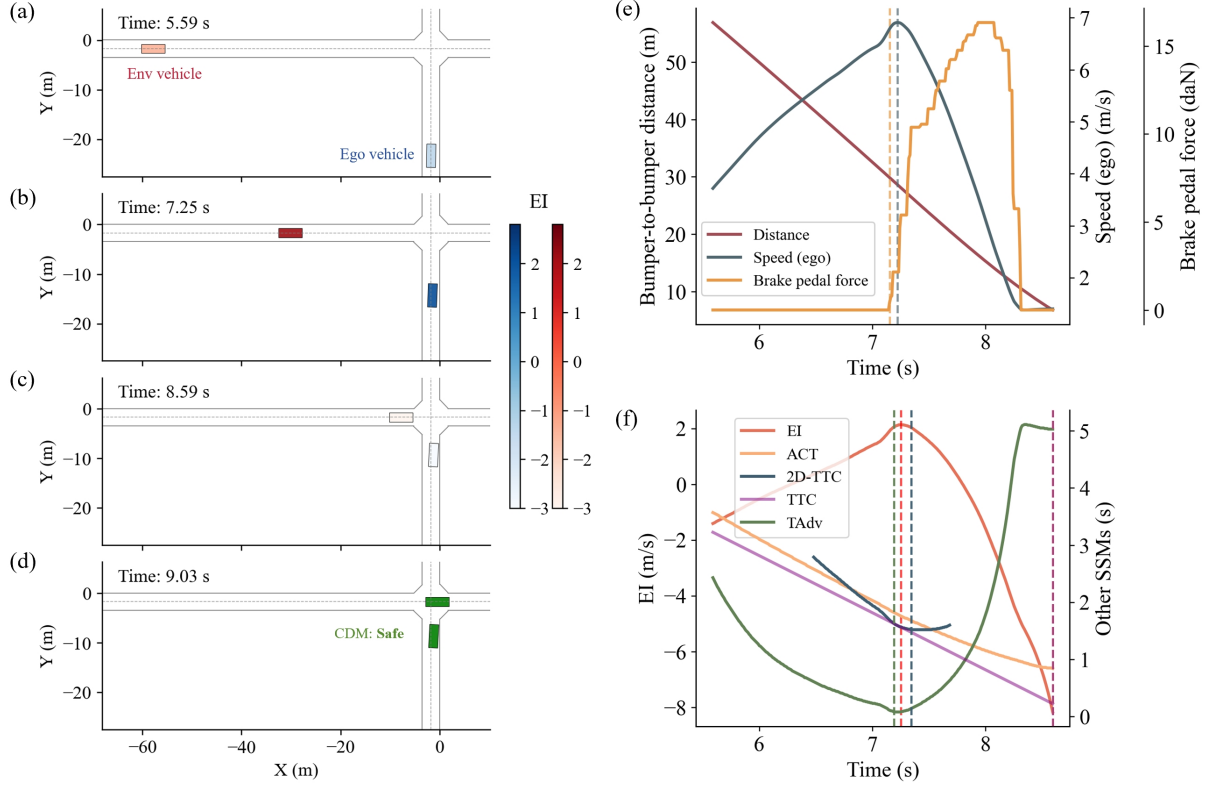


Figure 15: Scenario 3: Angle conflict. The ego vehicle brakes in time to avoid a collision. (a)-(d) Visualizations of the scene at different moments. (e) Profiles of the bumper-to-bumper distance, speed difference, and the ego vehicle’s brake pedal force over time. (f) Profiles of EI, ACT, 2D-TTC, TTC and TAdv over time.

Table 5: SSMs over time in scenario 3

Time (s)	P_1	P_2	EI (m/s)	ACT (s)	2D-TTC (s)	TTC (s)	TAdv (s)
5.59	✓	✓	-1.41	3.57	—	3.23	2.43
6.29	✓	✓	0.02	2.79	—	2.53	0.8
7.25	✓	✓	2.14	1.76	1.57	1.57	0.08
7.34	✓	✓	2.03	1.68	1.52	1.48	0.14
8.59	✓	✓	-8.17	0.84	—	0.22	5.03
9.03–9.19	✓	✗	—	—	—	—	—
≥ 9.20	✗	✗	—	—	—	—	—

Scenario 4: Head-on. This scenario depicts a two-way, two-lane head-on conflict, as shown in Figure 16. The vehicle on the left side is the ego vehicle, operated by a human driver, while the vehicle on the right side is the environment vehicle, controlled by a program setting in the simulation environment. Referring to Table 6, the description is as follows: Up to $t = 16.57$ s, condition P_1 is not met, detecting the situation as non-conflict. At $t = 16.58$ s, the environment vehicle develops a lateral speed, meeting conditions P_1 and P_2 and indicating a potential conflict. At $t = 16.90$ s, the driver initiates an evasive steering maneuver, with EI and TAdv peaking at 1.29 m/s and 0.01 s, respectively. At $t = 17.70$ s, 2D-TTC drops to its minimum of 1.01 s (beyond this time, the preconditions of 2D-TTC are not met). At $t = 17.99$ s, ACT reaches its minimum value of 0.98 s. After $t \geq 18.00$ s, the vehicles no longer meet condition P_1 . Overall, EI exhibits a pattern similar to TAdv, accurately representing the impact of evasive maneuvers on vehicle risk.

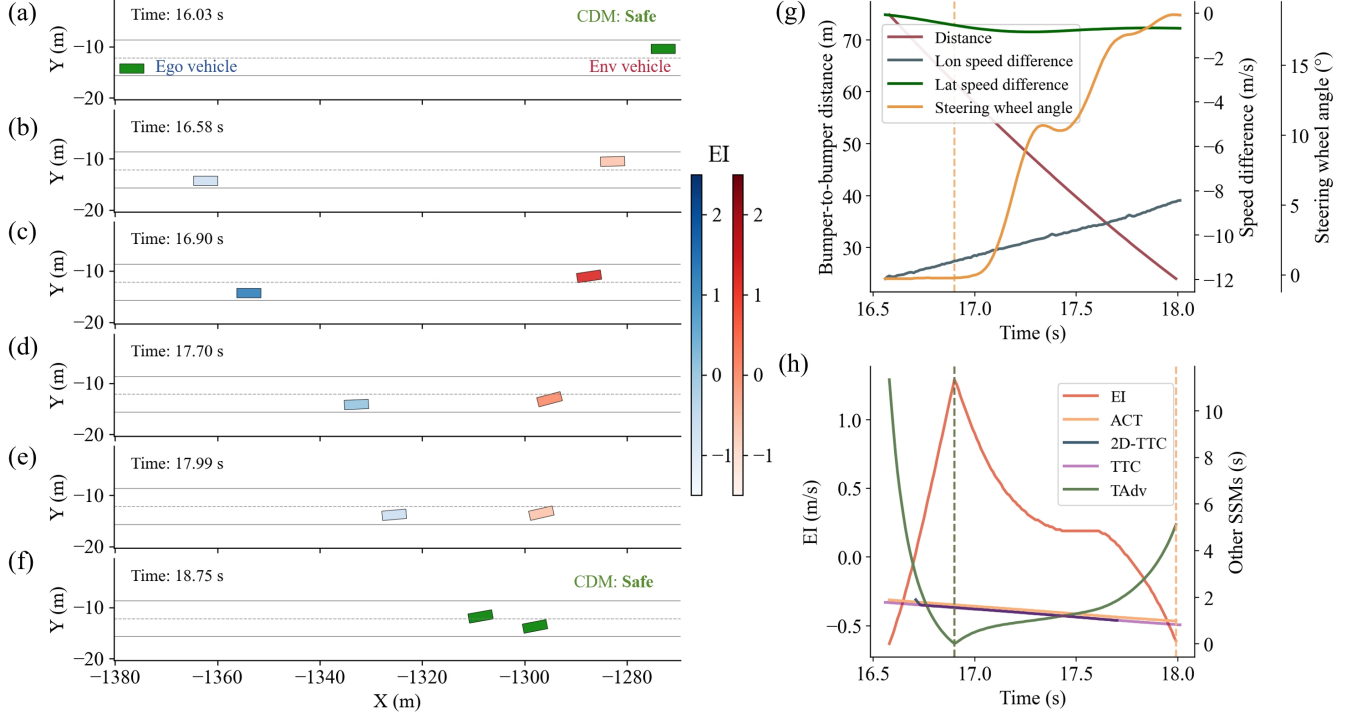


Figure 16: Scenario 4: Head-on conflict. On a two-way, two-lane road, the environment vehicle in the opposing lane loses control and swerves into the ego vehicle’s lane. The ego vehicle avoids a collision by executing a steering maneuver. (a)-(f) Visualizations of the scene at different moments. (g) Profiles of the bumper-to-bumper distance, speed difference, and the ego vehicle’s steering wheel angle over time. (h) Profiles of EI, ACT, 2D-TTC, TTC and TAdv over time.

Table 6: SSMs over time in scenario 4

Time (s)	P_1	P_2	EI (m/s)	ACT (s)	2D-TTC (s)	TTC (s)	TAdv (s)
≤ 16.57	×	✓	—	—	—	—	—
16.58	✓	✓	-0.63	1.89	—	1.77	11.34
16.90	✓	✓	1.29	1.68	1.56	1.56	0.01
17.70	✓	✓	0.09	1.15	1.01	1.01	1.86
17.99	✓	✓	-0.61	0.98	—	0.83	5.12
≥ 18.00	×	✓	—	—	—	—	—

Based on the four cases above, it is evident that EI behaves similarly to TTC in parallel conflicts and to TAdv in angle conflicts. Moreover, EI strongly correlates with drivers’ evasive maneuvers. Specifically, after a conflict occurs and before the driver begins evasive actions, EI gradually increases from negative to positive values, peaking around the time the driver starts the maneuver. After the maneuver, EI decreases and eventually turns negative. This indicates that if evasive maneuvers are delayed, the EI value will continue to rise until a collision occurs.

4.3. The impact of evasive maneuvers on EI

This section continues the discussion on the impact of evasive actions on EI and provides a new understanding of avoidance behaviors by drivers or collision avoidance systems for autonomous vehicles (AVs). An effective SSM must exhibit certain characteristics: (1) accurate conflict representation, as verified in section 4.2; (2) precise reflection of risk evolution, specifically how evasive actions influence risk. Preliminary conclusions indicate that EI is closely related to the vehicle’s evasive behaviors. The risk quantification of EI fundamentally focuses on two aspects: (1) the necessary adjustments for collision states, i.e., InDepth; (2) the time available for evasive actions, i.e., TDM.

To compare the impact of different evasive behaviors on EI, we set up an angle conflict scenario in a Python simulation environment. Based on the same initial risk condition, the starting InDepth is 2.35 m and the TDM is 3.38 s, as shown in Figure 17(a). Figure 17(a) depicts the scenario without any evasive maneuver, where the InDepth

remains positive and the EI value continuously increases as TDM decreases, leading up to a collision. Figure 17(b) shows the scenario where vehicle B takes an evasive maneuver; at $t=0.8$ s, vehicle B starts to brake, and the InDepth decreases to a negative value at $TDM=1.62$ s, thereby exiting the dangerous situation. The peak moment for EI occurs at $t=0.98$ s, with a maximum value of 0.95 m/s. Figure 17(c) illustrates cooperative evasion maneuvers by both vehicles; at $t=0.8$ s, vehicle B starts to brake while vehicle A begins to accelerate. The InDepth decreases to a negative value at $TDM=1.86$ s, exiting the danger. The peak moment for EI occurs at $t=0.88$ s, with a maximum value of 0.93 m/s.

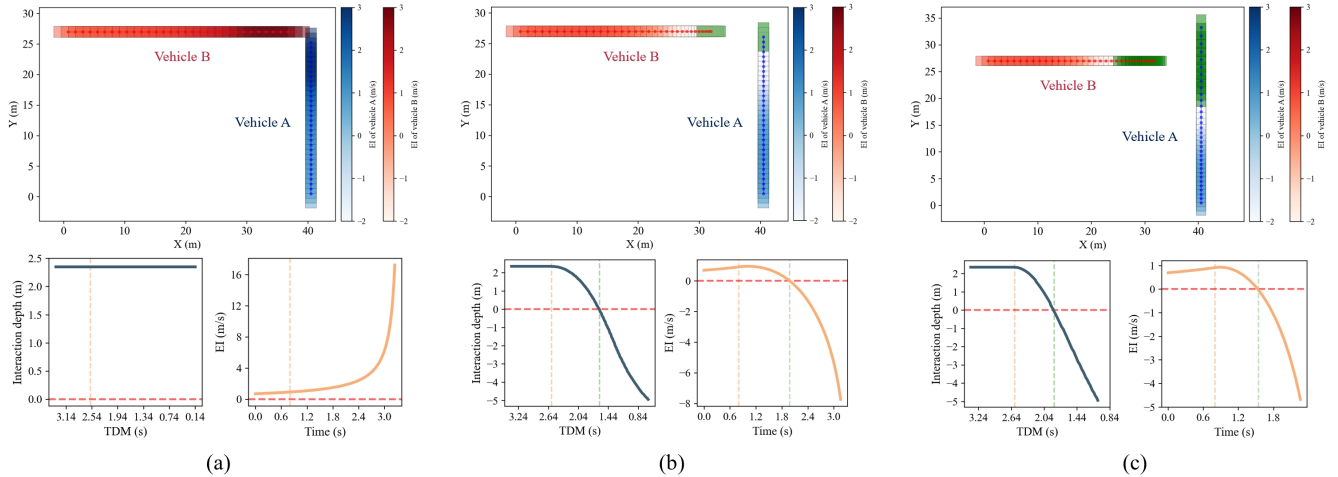


Figure 17: Simulation for the angle conflict scenario, comparing the impact of different evasive maneuvers on EI. (a) Without any evasive maneuvers. (b) Vehicle B takes an evasive maneuver. (c) Both vehicles engage in cooperative evasion actions.

Thus, EI provides a new understanding of evasive action. When facing imminent collision scenarios, the primary goal of drivers or AVs should be to reduce the InDepth between the two vehicles to a negative value before TDM decreases to 0, by executing appropriate evasive maneuvers. EI has the potential to serve as a real-time risk assessment module in driver assistance systems or collision avoidance systems. It can comprehensively detect potential vehicle risks, supervise evasive maneuvers in imminent collision scenarios, and thus enhance the safety of AVs.

4.4. Validation of real road data

After the case study, we further validate the accuracy of EI in representing risk using a large amount of real-world data. Since the true value of risk is “whether a collision occurs”, we extract a substantial amount of real conflict data and crash data to verify whether the proposed indicator can effectively differentiate between crash and conflict events.

The conflict data consists of two parts: urban and highway data. The urban conflict data is from the High-Speed Rail New City area in Suzhou, Jiangsu Province, China. Each intersection is equipped with four networked V2X roadside data collection devices, as shown in Figure 18. The sensors on each V2X device include LIDAR, gap-filling radar, and cameras. Data are transmitted in real-time to cloud servers via fiber optics, where they undergo data fusion and filtering processes. The data sampling rate is 10Hz, enabling the identification of each traffic participant’s information, including ID, centroid position, orientation angle, speed, length, width, and type. Road data are collected from intersections #2, #10, #11, and #20, with intersections #2 and #20 sampled separately and intersections #10 and #11 sampled together. The total data collection time exceeds 45 hours, involving 73,915 road users. The data includes vehicle conflicts within intersections as well as interactions before entering intersections due to merging and diverging behaviors. The highway conflict data is from the exiD dataset, which is recorded using camera-equipped drones at the entries and exits of the German Autobahn (Moers et al., 2022). This dataset contains 69,172 road users and includes over 16 hours of measurement data. Statistics show that the exiD dataset has a higher density of interactive and challenging scenarios compared to other highway datasets (e.g., the highHD dataset (Krajewski et al., 2018)). A summary of the conflict data collection is provided in Table 7.

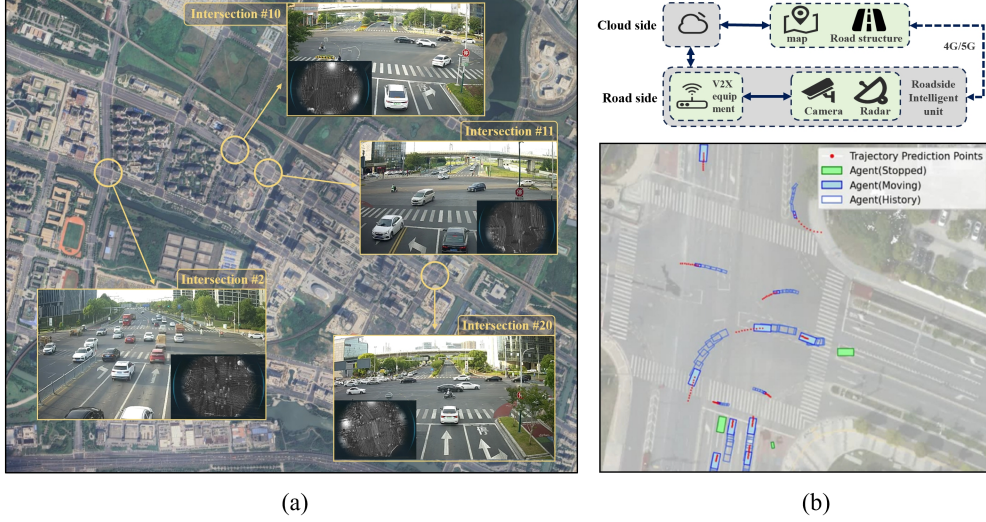


Figure 18: Data collection in Suzhou High-speed Rail New Town. (a) Map of the High-speed Rail New Town and the data collection intersections. (b) Data collection process.

Table 7: Conflict data for urban and highway driving scenarios

Sites	Hours	#Vehicles	#Conflict events
Suzhou, China (Urban)			
Intersection #2	≈15 h 40 min	20,257	32,473
Intersection #10 & 11	≈5 h 40 min	16,258	22,260
Intersection #20	≈24 h 00 min	37,400	25,694
German Autobahn (Highway)			
Aachen & Cologne (7 locations)	≈16 h 10 min	69,172	16,656

Due to the extremely low proportion of crash events in real road data, we used 69 urban and 30 highway vehicle-to-vehicle crash cases documented in (Zhao et al., 2019) as the crash data in our dataset. These data were provided by the Beijing Traffic Management Bureau and reconstructed based on crash responsibility determination reports. The complete processes of the crashes, including the collision phases, were restored to obtain full vehicle motion trajectories, speeds, and posture information, with a sampling frequency of 10Hz. The types of crashes in these data closely match those in the conflict data. Figure 19(b-c) shows the proportions of different road types and conflict types in both crash and conflict datasets.

We define positive samples as crash data and negative samples as conflict data. For each event, we calculate the values of EI and six typical SSMs, including ACT, 2D-TTC, TTC, TAdv, DRAC, and PET. We extract the maximum values of EI and DRAC, and the minimum values of the other SSMs, as the quantitative results representing the extreme risk level of each SSM for each event. ROC (Receiver Operating Characteristic) curves are utilized to validate the performance of different SSMs in classifying the samples, as shown in Figure 19(a). ROC curves depict the relationship between the True Positive Rate (TPR) and the False Positive Rate (FPR) at various threshold settings and are advantageous for handling class imbalance. The AUC (Area Under the Curve) is the area under the ROC curve, ranging from 0 to 1. The closer the AUC value is to 1, the better the classification effectiveness and robustness of the indicator. The AUC values for each SSM are shown in Figure 19(d).

The results show that the AUC value of EI is higher than that of ACT, 2D-TTC, TTC, TAdv, DRAC, and PET by 0.48%, 1.45%, 15.05%, 27.00%, 14.25%, and 32.05%, respectively. This indicates that EI's risk assessment results are closer to the true risk values in the real data. The superior performance of EI over ACT may be due to the following reasons: (1) TDM provides a more accurate estimation of temporal proximity; (2) considering InDepth offers a more fundamental 2D risk measure compared to methods that only consider single-directional

proximity. Since 2D-TTC takes into account risks in two directions, it performs better than TTC; however, 2D-TTC is less effective than ACT, suggesting that classifying conflicts solely into horizontal and vertical directions may have limitations when applied to multi-angle vehicle conflicts. TTC and DRAC are both widely used longitudinal proximity indicators, resulting in similar performance. TAdv theoretically could lead to false alarms, as it does not account for the time it takes vehicles to reach the conflict area; thus, two vehicles that are very far apart might still register a TAdv of 0, even if only minimal evasive action is required to avoid a collision. (Laureshyn et al., 2010) indicates that TAdv alone is insufficient to describe collision risk and should be used in conjunction with indicators such as TTC to provide a more effective representation of risk. PET is calculated based on the time difference between vehicles passing through the same road grid. This indicator depends on the road grid setup and may lead to some misjudgments. For instance, in certain collision cases, the two vehicles may bounce off in opposite directions after impact, making it difficult for the grid to capture shared occupancy in the same area and potentially even considering it risk-free. Conversely, if the grid area is set too large, two closely parallel-moving vehicles may be identified as a crash event. Figure 19(e) shows the box plots of the SSM distributions for positive samples (crashes) and negative samples (conflicts).

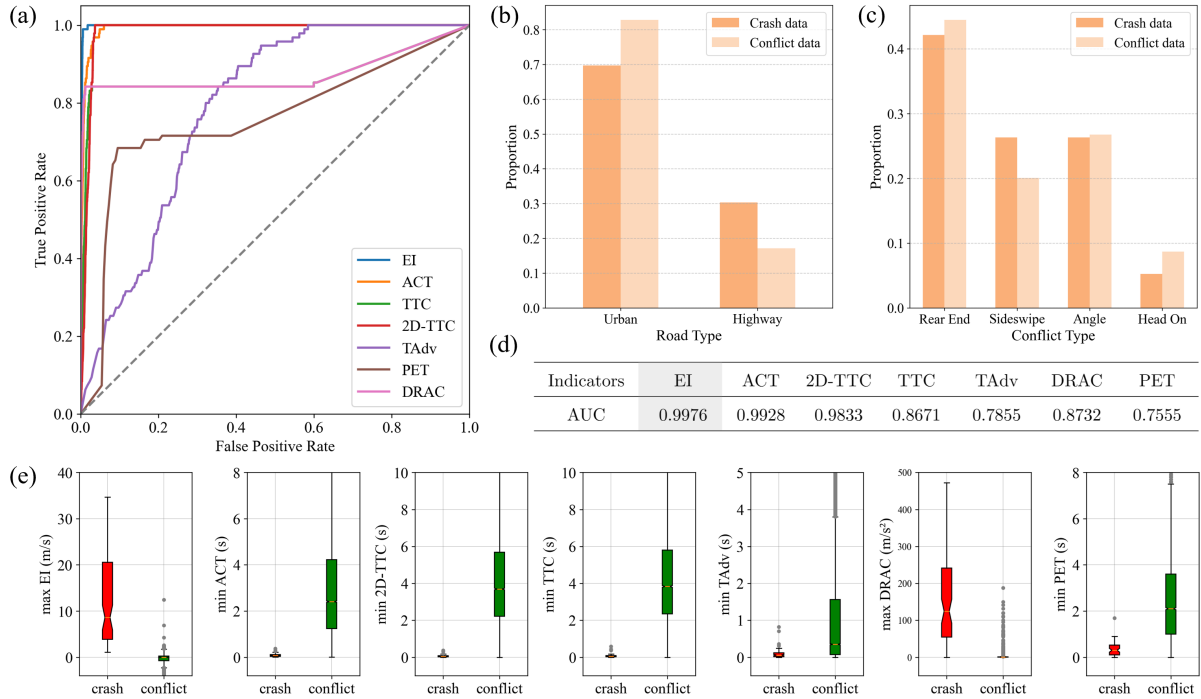


Figure 19: Results of different SSMs in crash-conflict classification. (a) ROC curves for different SSMs in crash-conflict classification. (b) Distribution of road types. (c) Distribution of conflict types. (d) AUC values for each SSM. (e) Box plots showing the distribution of EI and six other SSMs for crash data and conflict data.

4.5. Applications of EI in real-time road safety monitoring

To validate the potential of EI in real-time traffic safety systems, we deployed EI for real-time safety monitoring at intersections. Vehicle trajectory information is provided based on the SinD dataset (Xu et al., 2022), a high-precision trajectory dataset collected by drones in Tianjin, China, covering seven types of traffic participants and recording various traffic violations. For demonstration purposes, we select a subject vehicle (SV) in each scenario to monitor the risk posed by other road users toward it.

Safety monitoring Scenario 1. SV (Car #565) interacting with multiple two-wheelers while traveling straight, as shown in Figure 20(a). Between $t = 1259.1$ s and $t = 1266.5$ s, a total of 11 road users pass through the intersection. The CDM detects potential conflicts with a motorcycle and four bicycles, and then calculates the corresponding EI values for each conflict. The EI curve shows that at $t = 1260.4$ s, the conflict risk between the

SV and motorcycle #563 reaches its peak, with an EI value of 1.43 m/s. The SV initiates braking at $t = 1259.9$ s. At $t = 1263.2$ s, the conflict between the SV and motorcycle #563 is resolved, while bicycle #559 ahead of the SV reaches its peak risk at an EI value of 1.43 m/s. The SV accelerates at $t = 1262.3$ s, attempting to pass through the conflict zone ahead of the two bicycles. At $t = 1264.3$ s, the risk ranking for the two bicycles changes, with bicycle #560 representing the highest risk, and an EI value of 0.21 m/s. It is worth noting that, to avoid the risk posed by the two bicycles, the SV begins to execute lateral evasive maneuvers at $t = 1263.9$ s. At $t = 1266.1$ s, the CDM concludes that the SV has reached a safe state.

Safety monitoring Scenario 2. SV (Car #10) turning left and interacting with multiple types of road users, as shown in Figure 20(b). Between $t = 21.9$ s and $t = 30.0$ s, a total of 10 road users pass through the intersection. The CDM detects potential conflicts between the SV and one car, one bicycle, and two pedestrians. The EI curve shows that at $t = 23.3$ s, the SV has potential conflicts with Car #29, bicycle #27, and pedestrian #P8, with the highest risk observed with Car #29, where the EI value is 0.67 m/s. At $t = 24.9$ s, the sudden turn of bicycle #27 causes the risk between the SV and bicycle #27 to peak, with an EI value of 0.66 m/s. At $t = 26.3$ s, the conflict between the SV and bicycle #27 is resolved, while the EI value with Car #29 reaches 1.15 m/s. At $t = 27.5$ s, the SV gains a speed advantage and is able to pass Car #29 first, reducing the EI value with Car #29, while the risk with pedestrian #P11 ahead of the SV reaches its peak, with an EI value of 0.38 m/s. The SV's acceleration curve shows that at $t = 22.8$ s, the SV detects potential risk and initiates braking to create low-risk conditions for passing. At $t = 25.2$ s, the SV attempts to overtake Car #29 by accelerating.

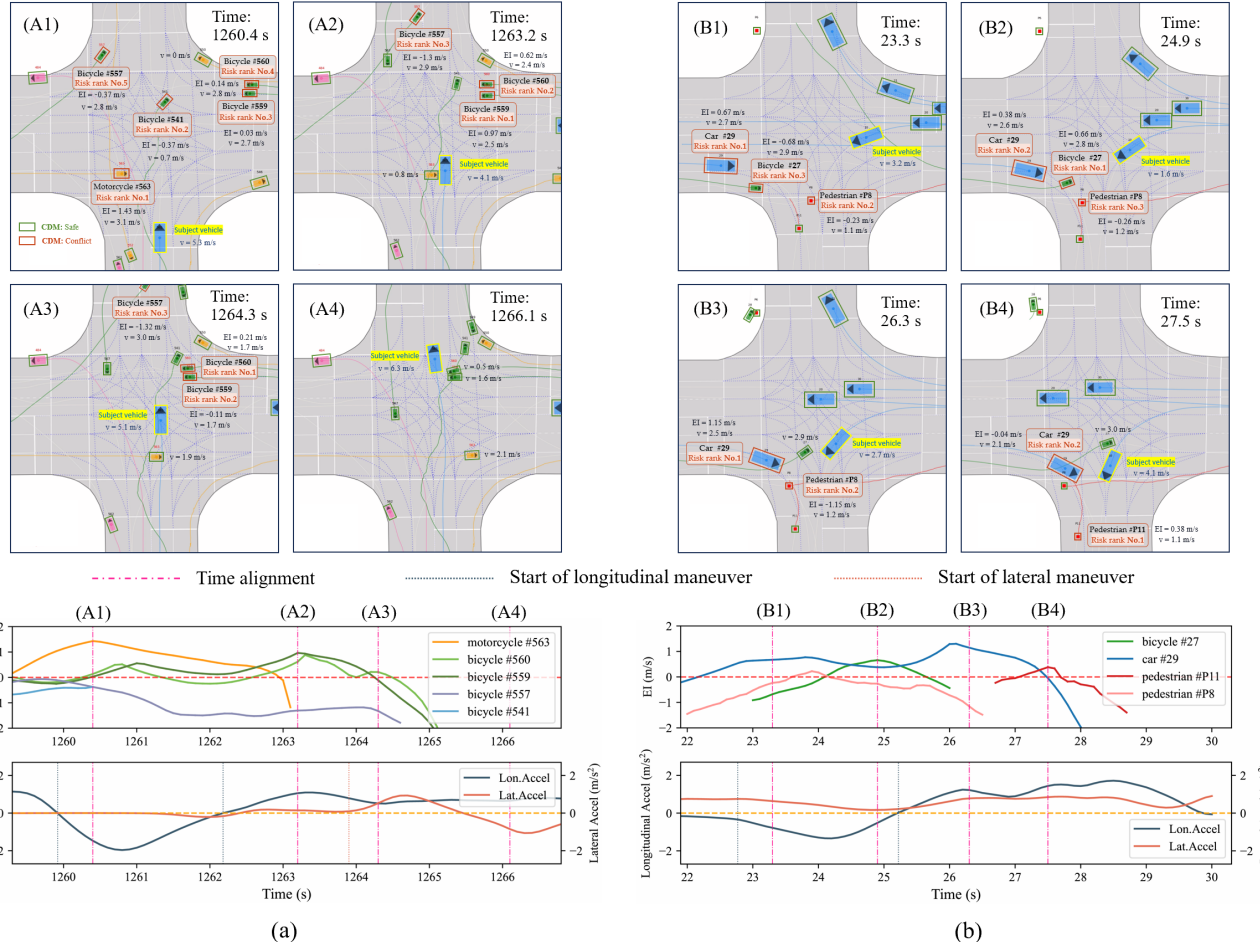


Figure 20: Real-time road safety monitoring through EI deployment. (a) Scenario 1: Subject vehicle (SV) interacting with multiple two-wheelers while traveling straight. (b) Scenario 2: SV turning left and interacting with multi-types of road users.

computation times for the two real-time safety monitoring cases are shown in Table 8. The CDM filters out

approximately two-thirds of non-risk road users in real time, allowing EI's risk-quantification component to focus on road users with potential conflicts with the SV. In scenarios with 8-9 surrounding vehicles, EI's processing time per frame is 3.91 ms, and with 11 vehicles, it is 5.08 ms, demonstrating EI's high computational efficiency and suitability for large-scale real-time traffic safety monitoring.

Table 8: Computation time analysis for EI in safety monitoring

Metrics	Scenario 1	Scenario 2
Average surrounding road users count per frame	11.01	8.51
Average conflict road users count per frame	4.84	2.05
CDM Per Frame Processing Time (ms)	2.60	2.32
Total EI safety monitoring per frame processing time (ms)	5.08	3.91

5. Conclusions

This paper proposes a novel SSM, Emergency Index (EI), which is independent of road topology and applicable to multi-angle conflict types in 2D plane. The Conflict Detection Model (CDM), as a precondition for EI, clearly defines the mathematical conditions for vehicles' potential conflicts. EI focuses on the predicted moment with the highest risk state, incorporating two aspects in its expression: the maximum depth at which both vehicles are projected to intrude into each other's safety region (i.e., InDepth), and the remaining time to reach this situation (i.e., TDM). The physical significance of EI lies in reflecting the intensity of the evasive actions required by both vehicles. Case studies show that the preconditions of EI are more general, effectively reducing the occurrence of missed detections. Experiments with driving simulators and simulations indicate that EI is consistent with the TTC and ACT in rear-end scenarios and aligns with TAdv in multi-angle conflict situations. Besides, EI demonstrates a strong correlation with evasive actions. Validation through extensive real road data reveals that the AUC values of EI are 0.48%, 1.45%, 15.05%, 27.00%, 14.25%, and 32.05%, higher than those of ACT, 2D-TTC, TTC, TAdv, DRAC, and PET, respectively. This suggests that EI's risk assessment results are closer to the true risk values of the real data and have a better capability of representing risk. For application, this paper demonstrates EI's computational efficiency and practical value by deploying it in real-time road safety monitoring scenarios.

The main advantages of the proposed method include:

1. CDM, as a precondition for the EI, enables comprehensive screening of potential conflict vehicles, reducing the occurrence of missed detections. CDM can be used as a universal precondition for other SSMs.
2. EI differs from the “combining indicator” method, as it has a clear physical meaning that reflects not only vehicle proximity but also the necessary adjustments between vehicle states, which integrates a multitude of conflict relationships within an interpretable risk assessment framework.
3. EI is distinct from existing TTC-based 2D-SSMs, as it moves beyond the limitations of traditional SSMs that rely on single-direction proximity measures, offering a new risk assessment framework for 2D-SSMs.
4. EI provides a new understanding of drivers' evasive actions. Specifically, two vehicles in danger should jointly take appropriate evasive maneuvers to change their InDepth to a negative value before the TDM reduces to zero; otherwise, the risk will further increase. Thus, EI represents the intensity of evasive action required by the two vehicles to avoid risk.

This study still has some limitations that can be addressed in future research. Firstly, the method proposed in this paper is based on the CV model as the predictive model. Future work should explore the impact of different predictive models on the evaluation of driving risk. Secondly, integrating vehicle dynamics models into the EI risk assessment framework is a topic worth exploring. Thirdly, refining the concept of the safety region could enhance the effectiveness and generalizability of EI, which requires extensive road testing and detailed calibration. Lastly, this study primarily focuses on vehicle conflicts; however, the applicability and validation of EI for vulnerable road users (VRUs) require further research.

Acknowledgment

This work is supported by the National Natural Science Foundation of China under Grant 52221005 and the Beijing Natural Science Foundation (No. 3244031). Additionally, the authors thank Prof. Hong Wang from Tsinghua University for her valuable contributions.

Code availability

Code availability is available at <https://github.com/AutoChengh/EmergencyIndex>.

References

- Allen, B. L., Shin, B. T., & Cooper, P. J. (1978). *Analysis of traffic conflicts and collisions*. Technical Report.
- Almqvist, S., Hyden, C., & Risser, R. (1991). Use of speed limiters in cars for increased safety and a better environment. *Transportation Research Record*, .
- Arun, A., Haque, M. M., Bhaskar, A., Washington, S., & Sayed, T. (2021). A systematic mapping review of surrogate safety assessment using traffic conflict techniques. *Accident Analysis & Prevention*, 153, 106016.
- Astarita, V., Guido, G., Vitale, A., & Giofré, V. (2012). A new microsimulation model for the evaluation of traffic safety performances, .
- Beauchamp, É., Saunier, N., & Cloutier, M.-S. (2022). Study of automated shuttle interactions in city traffic using surrogate measures of safety. *Transportation research part C: emerging technologies*, 135, 103465.
- Chan, C.-Y. (2006). Defining safety performance measures of driver-assistance systems for intersection left-turn conflicts. In *2006 IEEE Intelligent Vehicles Symposium* (pp. 25–30). IEEE.
- Charly, A., & Mathew, T. V. (2019). Estimation of traffic conflicts using precise lateral position and width of vehicles for safety assessment. *Accident Analysis & Prevention*, 132, 105264.
- Cunto, F. (2008). Assessing safety performance of transportation systems using microscopic simulation, .
- Feng, S., Sun, H., Yan, X., Zhu, H., Zou, Z., Shen, S., & Liu, H. X. (2023). Dense reinforcement learning for safety validation of autonomous vehicles. *Nature*, 615, 620–627.
- Guo, H., Xie, K., & Keyvan-Ekbatani, M. (2023). Modeling driver's evasive behavior during safety-critical lane changes: Two-dimensional time-to-collision and deep reinforcement learning. *Accident Analysis & Prevention*, 186, 107063.
- Hayward, J. C. (1972). Near miss determination through use of a scale of danger, .
- Hillenbrand, J., Spieker, A. M., & Kroschel, K. (2006). A multilevel collision mitigation approach—its situation assessment, decision making, and performance tradeoffs. *IEEE Transactions on intelligent transportation systems*, 7, 528–540.
- Hou, J., List, G. F., & Guo, X. (2014). New algorithms for computing the time-to-collision in freeway traffic simulation models. *Computational intelligence and neuroscience*, 2014, 761047.
- Huang, H., Zheng, X., Yang, Y., Liu, J., Liu, W., & Wang, J. (2020). An integrated architecture for intelligence evaluation of automated vehicles. *Accident Analysis & Prevention*, 145, 105681.
- Ismail, K., Sayed, T., & Saunier, N. (2011). Methodologies for aggregating indicators of traffic conflict. *Transportation research record*, 2237, 10–19.
- Jiao, Y., Calvert, S. C., Van Cranenburgh, S., & van Lint, H. (2023). Inferring vehicle spacing in urban traffic from trajectory data. *Transportation research part C: emerging technologies*, 155, 104289.
- Kar, P., Venturuthiyil, S. P., & Chunchu, M. (2023). Assessing the crash risk of mixed traffic on multilane rural highways using a proactive safety approach. *Accident Analysis & Prevention*, 188, 107099.
- Kesting, A., Treiber, M., & Helbing, D. (2010). Enhanced intelligent driver model to access the impact of driving strategies on traffic capacity. *Philosophical Transactions of the Royal Society A: Mathematical, Physical and Engineering Sciences*, 368, 4585–4605.
- Krajewski, R., Bock, J., Kloeker, L., & Eckstein, L. (2018). The highd dataset: A drone dataset of naturalistic vehicle trajectories on german highways for validation of highly automated driving systems. In *2018 21st international conference on intelligent transportation systems (ITSC)* (pp. 2118–2125). IEEE.
- Laureshyn, A., Svensson, Å., & Hydén, C. (2010). Evaluation of traffic safety, based on micro-level behavioural data: Theoretical framework and first implementation. *Accident Analysis & Prevention*, 42, 1637–1646.

- Mahmud, S. S., Ferreira, L., Hoque, M. S., & Tavassoli, A. (2017). Application of proximal surrogate indicators for safety evaluation: A review of recent developments and research needs. *IATSS research*, 41, 153–163.
- Minderhoud, M. M., & Bovy, P. H. (2001). Extended time-to-collision measures for road traffic safety assessment. *Accident Analysis & Prevention*, 33, 89–97.
- Moers, T., Vater, L., Krajewski, R., Bock, J., Zlocki, A., & Eckstein, L. (2022). The exid dataset: A real-world trajectory dataset of highly interactive highway scenarios in germany. In *2022 IEEE Intelligent Vehicles Symposium (IV)* (pp. 958–964). IEEE.
- Nikolaou, D., Ziakopoulos, A., & Yannis, G. (2023). A review of surrogate safety measures uses in historical crash investigations. *Sustainability*, 15, 7580.
- Organization, W. H. (2019). *Global action plan on physical activity 2018-2030: more active people for a healthier world*. World Health Organization.
- Ozbay, K., Yang, H., Bartin, B., & Mudigonda, S. (2008). Derivation and validation of new simulation-based surrogate safety measure. *Transportation research record*, 2083, 105–113.
- Peesapati, L. N., Hunter, M. P., & Rodgers, M. O. (2018). Can post encroachment time substitute intersection characteristics in crash prediction models? *Journal of safety research*, 66, 205–211.
- Perez, M. A., Sudweeks, J. D., Sears, E., Antin, J., Lee, S., Hankey, J. M., & Dingus, T. A. (2017). Performance of basic kinematic thresholds in the identification of crash and near-crash events within naturalistic driving data. *Accident Analysis & Prevention*, 103, 10–19.
- Salamati, K., Schroeder, B., Rouphail, N. M., Cunningham, C., Long, R., & Barlow, J. (2011). Development and implementation of conflict-based assessment of pedestrian safety to evaluate accessibility of complex intersections. *Transportation research record*, 2264, 148–155.
- Saunier, N., Sayed, T., & Ismail, K. (2010). Large-scale automated analysis of vehicle interactions and collisions. *Transportation Research Record*, 2147, 42–50.
- Saunier, N., Sayed, T., & Lim, C. (2007). Probabilistic collision prediction for vision-based automated road safety analysis. In *2007 IEEE Intelligent Transportation Systems Conference* (pp. 872–878). IEEE.
- Scanlon, J. M., Kusano, K. D., Daniel, T., Alderson, C., Ogle, A., & Victor, T. (2021). Waymo simulated driving behavior in reconstructed fatal crashes within an autonomous vehicle operating domain. *Accident Analysis & Prevention*, 163, 106454.
- Tafidis, P., & Pirdavani, A. (2023). Application of surrogate safety measures in higher levels of automated vehicles simulation studies: A review of the state of the practice. *Traffic injury prevention*, 24, 279–286.
- Tang, S., Lu, Y., Liao, Y., Cheng, K., & Zou, Y. (2024). A new surrogate safety measure considering temporal-spatial proximity and severity of potential collisions. *Applied Sciences*, 14, 2711.
- Tselentis, D. I., & Papadimitriou, E. (2023). Driver profile and driving pattern recognition for road safety assessment: Main challenges and future directions. *IEEE Open Journal of Intelligent Transportation Systems*, 4, 83–100.
- Van Winsum, W., Brookhuis, K. A., & de Waard, D. (2000). A comparison of different ways to approximate time-to-line crossing (tlc) during car driving. *Accident Analysis & Prevention*, 32, 47–56.
- Venthuruthiyil, S. P., & Chunchu, M. (2022). Anticipated collision time (act): A two-dimensional surrogate safety indicator for trajectory-based proactive safety assessment. *Transportation research part C: emerging technologies*, 139, 103655.
- Wang, C., Xie, Y., Huang, H., & Liu, P. (2021). A review of surrogate safety measures and their applications in connected and automated vehicles safety modeling. *Accident Analysis & Prevention*, 157, 106157.
- Wang, J., Wu, J., & Li, Y. (2015). The driving safety field based on driver–vehicle–road interactions. *IEEE Transactions on Intelligent Transportation Systems*, 16, 2203–2214.
- Ward, J. R., Agamennoni, G., Worrall, S., Bender, A., & Nebot, E. (2015). Extending time to collision for probabilistic reasoning in general traffic scenarios. *Transportation Research Part C: Emerging Technologies*, 51, 66–82.
- Xie, K., Yang, D., Ozbay, K., & Yang, H. (2019). Use of real-world connected vehicle data in identifying high-risk locations based on a new surrogate safety measure. *Accident Analysis & Prevention*, 125, 311–319.
- Xing, L., He, J., Abdel-Aty, M., Cai, Q., Li, Y., & Zheng, O. (2019). Examining traffic conflicts of up stream toll plaza area using vehicles' trajectory data. *Accident Analysis & Prevention*, 125, 174–187.
- Xu, Y., Shao, W., Li, J., Yang, K., Wang, W., Huang, H., Lv, C., & Wang, H. (2022). Sind: A drone dataset at signalized intersection in china. In *2022 IEEE 25th International Conference on Intelligent Transportation Systems (ITSC)* (pp. 2471–2478). IEEE.

- Yao, W., Zhao, H., Bonnifait, P., & Zha, H. (2013). Lane change trajectory prediction by using recorded human driving data. In *2013 IEEE Intelligent vehicles symposium (IV)* (pp. 430–436). IEEE.
- Zhao, Z.-g., Zheng, X.-j., Wang, J.-q., Xu, Q., & Kodaka, K. (2019). Assessing performance of collision mitigation brake system in chinese traffic environment. *Journal of Central South University*, 26, 2854–2869.
- Zheng, L., Ismail, K., & Meng, X. (2014). Traffic conflict techniques for road safety analysis: open questions and some insights. *Canadian journal of civil engineering*, 41, 633–641.